

Decoherence times of universal two-qubit gates in the presence of broad-band noise

E. Paladino,

Dipartimento di Fisica e Astronomia, Università di Catania and CNR IMM MATIS, Catania, C/O Viale Andrea Doria 6, Ed.10, 95125 Catania, Italy.

E-mail: epaladino@dmfci.unict.it

A. D'Arrigo,

Dipartimento di Fisica e Astronomia, Università di Catania and CNR IMM MATIS, Catania, C/O Viale Andrea Doria 6, Ed.10, 95125 Catania, Italy.

A. Mastellone,

C.I.R.A. Centro Italiano Ricerche Aerospaziali - Via Maiorise snc - 81043 Capua, Caserta, Italy.

G. Falci

Dipartimento di Fisica e Astronomia, Università di Catania and CNR IMM MATIS, Catania, C/O Viale Andrea Doria 6, Ed.10, 95125 Catania, Italy.

Abstract. Controlled generation of entangled states of two quantum bits is a fundamental step toward the implementation of a quantum information processor. In nano-devices this operation is counteracted by the solid-state environment, characterized by broadband and non-monotonic power spectrum often $1/f$ at low frequencies. For single qubit gates, incoherent processes due to fluctuations acting on different time scales result in peculiar short- and long-time behaviors. Markovian noise originates exponential decay with relaxation and decoherence times, T_1 and T_2 , simply related to the symmetry of the qubit-environment coupling Hamiltonian. Noise with $1/f$ power spectrum at low frequencies is instead responsible for defocusing processes and algebraic short-times behavior. In this article we identify the relevant decoherence times of an entangling operation due to the different decoherence channels originated from solid state noise. Entanglement is quantified by the concurrence, which we evaluate in analytic form employing a multi-stage approach. "Optimal" operating conditions of reduced sensitivity to noise sources are identified. We apply this analysis to a superconducting $\sqrt{i - \text{SWAP}}$ gate for experimental noise spectra.

PACS numbers: 03.65.Yz, 03.67.Lx, 85.25.-j, 05.40.-a

1. Introduction

The implementation of a universal two-qubit gate involving an entanglement operation on two quantum bits represents a necessary step toward the construction of a scalable quantum computer [1]. Intense research on solid state nano-devices during the last decade has established the possibility to combine quantum coherent behavior with the existing integrated-circuit fabrication technology. In particular, based on superconducting technologies, a variety of high-fidelity single qubit gates are nowadays available [2, 3, 4], two-qubit logic gates [5, 6] and violations of Bell's inequalities [7] have been demonstrated, high-fidelity Bell states generated [8]. The recent demonstrations of simple quantum algorithms [9] and three-qubit entanglement [10] are further important steps toward a practical quantum computation with superconducting circuits.

The requirements for building an elementary quantum processor are however quite demanding on the efficiency of the protocols. This includes both a severe constraint on readout and a sufficient isolation from fluctuations to reduce decoherence effects. Solid-state noise sources are often characterized by broad-band and non-monotonic power spectrum. Similar noise characteristics have been reported in implementations based on Cooper-pair-boxes (CPB) [11, 12, 13], in persistent current [14] and phase qubits [15, 16]. Usually, the spectrum of at least one of the noise sources is $1/f$ at low-frequencies [12, 14, 17, 18, 19, 20]. At the system's eigen-frequencies instead (5 – 15 GHz) indirect measurements indicate white or ohmic spectrum [12, 13, 14]. Sometimes spurious resonances of various physical origin have been observed [15, 16, 21].

At the single-qubit level, the effects of the environmental degrees of freedom responsible for the various parts of the spectrum have been clearly identified leading to a convenient classification in terms of *quantum noise* and *adiabatic noise* effects [13, 22]. Understanding how these mechanisms affect an entanglement-generating two-qubit gate is a relevant issue not yet investigated and it is the subject of the present article.

The picture for a single qubit can be summarised as follows. Noise at frequencies of the order of the system's splittings may induce incoherent energy exchanges between qubit and environment (*quantum noise*). Relaxation processes occur only if the qubit-environment interaction induces spin flips in the qubit eigenbasis, i.e. for transverse noise. Weakly-coupled Markovian noise can be treated by a Born-Markov master equation [23]. It leads to relaxation and decoherence times denoted respectively T_1 and T_2 in Nuclear Magnetic Resonance (NMR) [24]. For transverse noise they are related by $T_2 = 2T_1$. Longitudinal noise does not induce spin flips, but it is responsible for pure dephasing with a decay-time denoted T_2^* [24]. In general, both relaxation and pure dephasing processes occur and the resulting decoherence time is $T_2 = [1/(2T_1) + 1/T_2^*]^{-1}$.

Since quantum measurements require averages of measurements runs, the main effect of fluctuations with $1/f$ spectrum is defocusing, similarly to inhomogeneous broadening in NMR [24]. Fluctuations with large spectral components at low frequencies can be treated as stochastic processes in the adiabatic approximation (*adiabatic noise*). The short-times decay of qubit coherences depends on the symmetry of the qubit-

environment coupling Hamiltonian. For transverse noise, the time dependence is algebraic $\propto [1 + at^2]^{-1/4}$, for longitudinal noise it is exponential quadratic $\propto \exp(-bt^2)$ ("static-path" [22] or "static-noise" [13] approximation).

The simultaneous presence of adiabatic and quantum noise can be treated in a multi-stage approach [22]. In simplest cases, the effects of the two noise components add up independently in the coherences time-dependence. Defocusing is minimized when noise is transverse with respect to the qubit Hamiltonian [11]. The qubit is said to operate at an "optimal point" characterised by algebraic short-times behavior followed by exponential decay on a scale $2T_1$.

In the present article we perform a systematic analysis of the effects and interplay of adiabatic and quantum noise on a universal two-qubit gate, extending the multi-stage elimination approach introduced in ref. [22]. Understanding these effects is crucial in the perspective of implementing solid-state complex architectures. Our system consists of two coupled qubits each affected by transverse and longitudinal noise with broad-band and non-monotonic spectrum. Such a general situation has not being studied in the literature. Previous studies concentrated on harmonic baths with monotonic spectrum relying on master equation and/or perturbative Redfield approach [25], or on numerical methods [26], or on formal solutions for selected system observables [27].

We quantify entanglement via the concurrence [28]. To compare with bit-wise measurements, single qubit switching probabilities are also evaluated. Our analysis is based on approximate analytic results and exact numerical simulations. Our main results are: (i) The identification of characteristic time scales of entanglement decay due to adiabatic noise, quantum noise and their interplay; (ii) The characterization of relaxation and dephasing for an entanglement operation via the time scales T_R , T_1^{SWAP} , T_2^{SWAP} and T_2^{SWAP*} . We point out the dependence of these scales on the symmetry of the Hamiltonian describing the interaction between each qubit and the various noise sources; (iii) The demonstration that a universal two-qubit gate can be protected against noise by operating at an "optimal coupling", extending the concept of single-qubit "optimal point".

The article is organized as follows. In Section 2 we introduce the Hamiltonian model for two-qubit entanglement generation in the presence of independent noise sources affecting each unit. In Section 3 the general features of the power spectra of these fluctuations, as observed in single qubit experiments, are summarized. The relevant dynamical quantities are introduced and the multi-stage approach to eliminate noise variables and obtain a reduced description of the two-qubit system is illustrated. In Sections 4 and 5 we derive separately the effect of quantum noise within a master equation approach and the leading order effect (quasi-static approximation) of adiabatic noise. Finally, in Section 6 we discuss their interplay and introduce the relevant time scales characterizing loss of coherence and entanglement of a universal two-qubit gate in a solid-state environment. Results are summarized in table 5 and in table 6. In Appendix A the entanglement generating model is derived for capacitive coupled Cooper Pair Boxes (CPBs) including fluctuations of all control parameters. In Appendix B

Table 1. Eigenvalues and eigenvectors of \mathcal{H}_0 expressed in the computational basis $|\mu\nu\rangle \equiv |\mu\rangle_1 \otimes |\nu\rangle_2$, $\mu, \nu \in \{+, -\}$ with $\sigma_{\alpha z}|\pm\rangle_\alpha = \mp|\pm\rangle_\alpha$ and $\tan \varphi = -\omega_c/(2\Omega)$.

i	ω_i	$ i\rangle$
0	$-\sqrt{\Omega^2 + (\omega_c/2)^2}$	$-(\sin \varphi/2) ++\rangle + (\cos \varphi/2) --\rangle$
1	$-\omega_c/2$	$(- +-\rangle + -+\rangle)/\sqrt{2}$
2	$\omega_c/2$	$(+-\rangle + -+\rangle)/\sqrt{2}$
3	$\sqrt{\Omega^2 + (\omega_c/2)^2}$	$(\cos \varphi/2) ++\rangle + (\sin \varphi/2) --\rangle$

the effect of selected impurities strongly coupled to the device is pointed out and we speculate on the possibility to extend the "optimal coupling" scheme under these conditions.

2. Universal entangling gate

Entanglement-generating two qubit gates have been implemented based on different coupling strategies. In the standard idea of gate-based quantum computation, the coupling between the qubits is switched on for a quantum gate operation and switched off after it. The easiest way to realize this scheme is to tune the qubits in resonance with each other for efficient coupling and move them out of resonance for decoupling. Employing a fixed coupling scheme two-qubit logic gates have been implemented [5] and high-fidelity Bell states have been generated in capacitive coupled phase qubits [8]. A different idea is to introduce an extra element between the qubits: an adjustable coupler, which can turn the coupling on and off [29, 30]. Alternatively, two-qubit gates are generated by applying microwave signals of appropriate frequency, amplitude and phase [31].

The core of the entangling operation of most of the above coupling schemes consists of two resonant qubits with a coupling term transverse with respect to the qubits quantization axis, as modeled by

$$\mathcal{H}_0 = -\frac{\Omega}{2} \sigma_{1z} \otimes \mathbb{I}_2 - \frac{\Omega}{2} \mathbb{I}_1 \otimes \sigma_{2z} + \frac{\omega_c}{2} \sigma_{1x} \otimes \sigma_{2x}. \quad (1)$$

Here $\sigma_{\alpha z}$ are Pauli matrices and \mathbb{I}_α is the identity, in qubit- α Hilbert space ($\alpha = 1, 2$). In our notation, $\sigma_{\alpha z}$ is the qubit- α quantization axis and we put $\hbar = 1$. This model applies in particular to the fixed, capacitive or inductive, coupling of superconducting qubits [32], where individual-qubit control allows an effective switch on/off of the interaction.

Eigenvalues and eigenvectors of eq. (1) are reported in table 1. In order to maintain the single qubit identities, the coupling strength, ω_c , must be one-to-two orders of magnitudes smaller than the single qubit level spacing, Ω . Thus eigenvalues form a doublets structure, as schematically illustrated in figure 1. The Hilbert space factorizes in two subspaces spanned by $\{|1\rangle, |2\rangle\}$ and $\{|0\rangle, |3\rangle\}$. A couple of qubits described by (1) is suitable to demonstrate entanglement generation. The system prepared in the

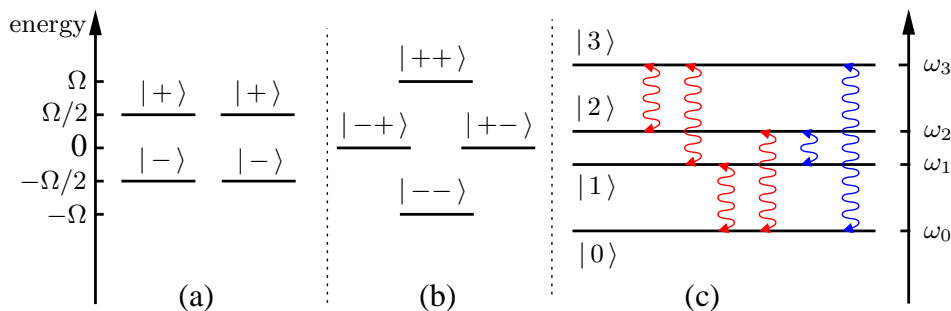


Figure 1. (a) Eigenenergies of the uncoupled resonant qubits; (b) levels in the two-qubit Hilbert space and logic basis of product states. (c) When the coupling is turned on the states $|+-\rangle$ and $|-+\rangle$ mix and an energy splitting $\omega_c \ll \Omega$ develops between the eigenstates $\{|2\rangle, |1\rangle\}$, spanning the SWAP subspace. Product states $|--\rangle$ and $|++\rangle$ weakly mix and split, with $\omega_3 - \omega_0 = 2\sqrt{\Omega + (\omega_c/2)^2}$. The eigenstates $\{|0\rangle, |3\rangle\}$ span the Z subspace. Longitudinal noise in the computational basis is responsible for inter-doublet relaxation processes (effective transverse inter-doublet) indicated by red wavy lines (Eq. (7)). Transverse noise in the computational basis originates incoherent energy exchanges inside each subspace (effective transverse intra-doublet) indicated by blue wavy lines (Eqs. (5), (6)).

factorized state $|+-\rangle$ freely evolves to the entangled state $|\psi_e\rangle = [|+-\rangle - i|-+\rangle]/\sqrt{2}$ in a time $t_e = \pi/2\omega_c$, realizing a $\sqrt{i - \text{SWAP}}$ operation. The dynamics takes place inside the $\{|1\rangle, |2\rangle\}$ subspace, which we name "SWAP-subspace". The orthogonal subspace will be instead named "Z-subspace".

Fluctuations of the control parameters used for the manipulation of individual qubits couple the circuit to environmental degrees of freedom. We consider the general situation where each qubit is affected both by longitudinal noise (coupled to $\sigma_{\alpha z}$) and by transverse noise (coupled to $\sigma_{\alpha x}$), as described by the interaction Hamiltonian

$$\mathcal{H}_I = -\frac{1}{2} [\hat{x}_1 \sigma_{1x} + \hat{z}_1 \sigma_{1z}] \otimes \mathbb{I}_2 - \frac{1}{2} \mathbb{I}_1 \otimes [\hat{x}_2 \sigma_{2x} + \hat{z}_2 \sigma_{2z}]. \quad (2)$$

Here \hat{x}_α and \hat{z}_α are collective environmental quantum variables coupled to different qubits degrees of freedom. For instance, in the case of two CPB-based qubits at the charge optimal point [3], the charge operator is $\sigma_{\alpha x}$, and the Josephson operator is $\sigma_{\alpha z}$. Fluctuations of the gate charge are described by a transverse coupling term, $\hat{x}_\alpha \sigma_{\alpha x}$, and noise in the superconducting phase by the longitudinal term, $\hat{z}_\alpha \sigma_{\alpha z}$ [13] (see Appendix A for the derivation) ‡. The complete device Hamiltonian reads $\mathcal{H}_0 + \mathcal{H}_I + \mathcal{H}_R$, where \mathcal{H}_R denotes the free Hamiltonian of all environmental variables.

In order to identify relaxation and pure dephasing processes for the coupled qubit setup we project $\mathcal{H}_0 + \mathcal{H}_I$ in the 4-dim Hilbert space generated by the eigenstates of \mathcal{H}_0 ,

‡ In our notation the qubit's quantization axis is $\sigma_{\alpha z}$, irrespective of the working point. Thus, \hat{x}_α and \hat{z}_α describe physically different processes only at selected operating points. Usually, this is the case at the single qubit's optimal points, see Appendix A.

$\{|i\rangle\}$, $i = 0, 1, 2, 3$, where we may rewrite

$$\begin{aligned}
 \mathcal{H}_0 &= \sum_i \omega_i |i\rangle\langle i| = \frac{\omega_c}{2} [|2\rangle\langle 2| - |1\rangle\langle 1|] + \sqrt{\Omega^2 + (\omega_c/2)^2} [|3\rangle\langle 3| - |0\rangle\langle 0|] \quad (3) \\
 \mathcal{H}_I &= \frac{1}{2}(\hat{x}_1 + \hat{x}_2) [A_-|2\rangle\langle 0| + A_+|2\rangle\langle 3| + \text{h.c.}] + \\
 &+ \frac{1}{2}(\hat{x}_1 - \hat{x}_2) [-A_+|1\rangle\langle 0| + A_-|1\rangle\langle 3| + \text{h.c.}] \\
 &- \frac{1}{2}(\hat{z}_1 - \hat{z}_2) [|1\rangle\langle 2| + |2\rangle\langle 1|] \\
 &- \frac{1}{2}(\hat{z}_1 + \hat{z}_2) [\cos \varphi (|0\rangle\langle 0| - |3\rangle\langle 3|) + \sin \varphi (|0\rangle\langle 3| + |3\rangle\langle 0|)] \quad (4)
 \end{aligned}$$

where $A_{\pm} = [\cos(\varphi/2) \pm \sin(\varphi/2)]/\sqrt{2}$, with $\tan \varphi = -\omega_c/(2\Omega)$. In (4) we distinguish "effective longitudinal" and "effective transverse" terms. The first ones are diagonal in the eigenbasis $\{|i\rangle\}$ and are responsible for pure dephasing processes. "Effective transverse" terms instead are off-diagonal and originate both intra- and inter-doublet relaxation processes. Specifically we have:

SWAP subspace $\{|1\rangle, |2\rangle\}$: Longitudinal noise in the computational basis $\propto \sigma_{\alpha z} \hat{z}_{\alpha}$, originates "effective transverse" noise in the SWAP-subspace, i.e. the restriction of $\mathcal{H}_0 + \mathcal{H}_I$ to $\{|1\rangle, |2\rangle\}$ reads

$$\mathcal{H}_{SWAP}^{proj} = \frac{\omega_c}{2} [|2\rangle\langle 2| - |1\rangle\langle 1|] - \frac{1}{2}(\hat{z}_1 - \hat{z}_2) [|1\rangle\langle 2| + |2\rangle\langle 1|] \quad (5)$$

Note that if both qubits were affected by the same longitudinal noise no effective transverse noise in this subspace would be present. This situation may occur in the presence of totally correlated noise affecting both qubits [33].

Z subspace $\{|0\rangle, |3\rangle\}$: Longitudinal noise in the computational basis originates both "effective transverse" and "effective longitudinal" noise in the Z-subspace, i.e. the projection of $\mathcal{H}_0 + \mathcal{H}_I$ on $\{|0\rangle, |3\rangle\}$ reads

$$\begin{aligned}
 \mathcal{H}_Z^{proj} &= \sqrt{\Omega^2 + (\omega_c/2)^2} [|3\rangle\langle 3| - |0\rangle\langle 0|] \\
 &+ (\hat{z}_1 + \hat{z}_2) [\cos \varphi (|0\rangle\langle 0| - |3\rangle\langle 3|) + \sin \varphi (|0\rangle\langle 3| + |3\rangle\langle 0|)]. \quad (6)
 \end{aligned}$$

Effective longitudinal and transverse components are modulated via the mixing angle, φ , similarly to a single qubit with operating point φ .

Inter-doublet processes: The only effect of transverse noise in the computational basis is to mix the two subspaces via "effective transverse" inter-doublet terms (Fig.1 (c))

$$\begin{aligned}
 \mathcal{H}_{inter} &= \frac{1}{2}(\hat{x}_1 + \hat{x}_2) [A_-|2\rangle\langle 0| + A_+|2\rangle\langle 3| + \text{h.c.}] \\
 &+ \frac{1}{2}(\hat{x}_1 - \hat{x}_2) [-A_+|1\rangle\langle 0| + A_-|1\rangle\langle 3| + \text{h.c.}] \quad (7)
 \end{aligned}$$

These inter-doublet terms are responsible, in particular, for relaxation processes from the SWAP-subspace to the ground state. We will demonstrate that the resulting "global" relaxation time sets the upper limit to all other gate operation times, including other decoherence time scales.

3. Multi-scale approach to broad-band noise

The considered entanglement generating operation takes place in the presence of broad-band and non-monotonic noise. In this Section we review the multi-stage elimination approach to deal with this problem. The method has been introduced for a single qubit in ref. [22] where the various approximations have been checked by comparing with the exact numerical solution of the system evolution. This approach allowed to accurately explain the observed dynamics in different experiments [13, 14], confirming its appropriateness to deal with the more complex system studied in the present article. The method has been extended to a multi-qubit gate in ref. [34], here we summarize the main steps.

The multi-stage elimination approach is based on a classification of the noise sources according to their effects and circumvents the problem of a microscopic description of noise sources, which are often non Gaussian and non Markovian [35, 36]. In this perspective, the required statistical information on the environment depends on the specific quantum operation performed and on the measurement protocol. Even if the statistical characterization of the environment requires going beyond the second order cumulant, often knowledge of the power spectrum of the bath variables, here \hat{x}_α and \hat{z}_α denoted generically as \hat{E}_α ,

$$S_{E_\alpha}(\omega) = \frac{1}{2} \int_0^{+\infty} dt e^{-i\omega t} [\langle\langle \hat{E}_\alpha(t) \hat{E}_\alpha(0) \rangle\rangle + \langle\langle \hat{E}_\alpha(0) \hat{E}_\alpha(t) \rangle\rangle], \quad (8)$$

is sufficient. Where $\langle\langle \dots \rangle\rangle$ denotes the equilibrium average with respect to \mathcal{H}_R and we assumed stationary processes with $\langle\langle \hat{E}_\alpha \rangle\rangle = 0$. The typical power spectrum reported in various single qubit experiments is sketched in figure 2. To make explicit reference to some practical situations, in table 2 we summarize the characteristics of transverse and longitudinal noise spectra at low- and high-frequencies reported in a CPB-based circuit [13] and in the recent experiment on a flux qubit [14].

The low-frequency part of the spectra of each variable is $1/f$, $S_{E_\alpha}^{1/f}(\omega) = A_{E_\alpha}/\omega$. The amplitude A_{E_α} can be estimated from spectral measurements. If γ_m and γ_M denote respectively the low- and high-frequency cut-offs of the $1/f$ region, then $A_{E_\alpha} = \pi \sigma_{E_\alpha}^2 [\ln(\gamma_M/\gamma_m)]^{-1}$, where $\sigma_{E_\alpha}^2$ is the variance, $\sigma_{E_\alpha}^2 = \int_{\gamma_m}^{\gamma_M} \frac{d\omega}{\pi} S_{E_\alpha}^{1/f}(\omega)$. It can be approximated as $\sigma_{E_\alpha}^2 = \int_{1/t_m}^{\gamma_M} \frac{d\omega}{\pi} S_{E_\alpha}^{1/f}(\omega)$ where t_m is the overall acquisition time for a single data point which results from averaging over several measurement trials. §

The high-frequency power spectrum is usually inferred indirectly from measurements of the qubit relaxation times under various protocols [12, 13, 14]. From the resulting figures the expected spectra for the corresponding quantum variables \hat{E}_α at the relevant frequencies, $\Omega/2\pi$ and $\omega_c/2\pi$ are derived. Experiments tuning the single qubit level spacing Ω reveal either ohmic [12, 14] or white [13] power spectrum in the

§ The intrinsic high-frequency cut-off of the $1/f$ spectrum depends on the specific microscopic source and it is usually not detectable in experiments. In the present article we discuss measurements protocols where the details of the behavior of the power spectrum below γ_m and around γ_M are not relevant and results depend logarithmically on the ratio γ_M/γ_m .

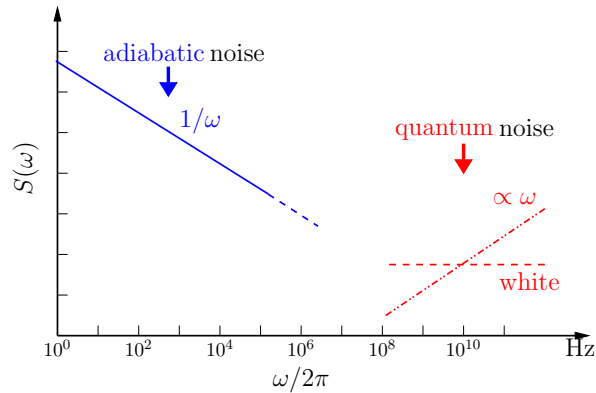


Figure 2. Sketch of the typical power spectrum of the environmental variable \hat{E}_α (logarithmic scale). Measurements of $1/f$ noise usually extend between 1 Hz and 0.1 – 1 MHz, whereas the ohmic or white spectrum region typically ranges around 5 – 20 GHz [13, 14]. The region classified as adiabatic noise and quantum noise are indicated.

Table 2. Characteristics of transverse and longitudinal noise at low- and high-frequencies inferred from data reported in ref.[3] for a charge-phase qubit at its double optimal point with $\Omega \approx 2\pi \times 16\text{GHz}$ (charge noise is transverse and phase noise is longitudinal), and in ref.[14] for a flux qubit at the optimal point with $\Omega \approx 2\pi \times 5\text{GHz}$ (flux noise is transverse and critical current noise is longitudinal). For the charge-phase qubit we considered $\gamma_M/\gamma_m = 10^6$, results logarithmically depend on this ratio.

	Charge-Phase Qubit	Flux Qubit
$S_x^{1/f}$	$\sigma_x \approx 2 \times 10^{-2} \Omega$	$\sigma_x \approx 2 \times 10^{-3} \Omega$
$S_z^{1/f}$	$\sigma_z \approx 10^{-6} \Omega$	$\sigma_z \approx 10^{-5} \Omega$
S_x	$S_x(\Omega) \approx 4 \times 10^6 \text{ s}^{-1}$	$S_x(\Omega) \approx 2 \times 10^5 \text{ s}^{-1}$
S_z	$S_z(\Omega) \approx 10^5 \text{ s}^{-1}$	-

GHz range. Evidence of spurious resonances in the spectrum have often been reported, they show up as beatings in time resolved measurements [3, 16].

In our analysis noise sources belong to three classes. Low frequency noise with $1/f$ spectrum is adiabatic since it does not induce transitions, but mainly defocuses the signal, we classify it as *adiabatic noise*. Noise at frequencies of the order of the qubits splittings is responsible for dissipation and ultimately for spontaneous decay, thus it is classified as *quantum noise*. Possible resonances in the spectrum pertain to the class named *strongly coupled noise*. Noise sources belonging to different classes act on different frequency scales and are treated via specific approximation schemes. The distinction can be illustrated as follows. We are interested to a reduced description of the 2-qubit system, expressed by the reduced density matrix (RDM), $\rho(t)$ obtained by tracing out environmental degrees of freedom from the total density matrix $\rho^{\text{Q,A,SC}}(t)$, which depends on quantum (Q), adiabatic (A) and strongly coupled (SC) bath variables. Since bath's degrees of freedom belonging to different classes of noise act of different

time scales we separate in each part of the interaction Hamiltonian, $\sigma_{\alpha i} \hat{E}_\alpha$ ($i = x, z$), the contribution from various noise classes as follows

$$\sigma_{\alpha i} \hat{E}_\alpha \rightarrow \sigma_{\alpha i} \hat{E}_\alpha^{\text{Q}} + \sigma_{\alpha i} \hat{E}_\alpha^{\text{A}} + \sigma_{\alpha i} \hat{E}_\alpha^{\text{SC}}. \quad (9)$$

Adiabatic noise, $\hat{E}_\alpha^{\text{A}}$, is typically correlated on a time scale much longer than the inverse of the qubit's frequencies, Ω_α , then in the spirit of the Born-Oppenheimer approximation it can be seen as a classical stochastic field $\{E_\alpha(t)\} \equiv \vec{E}(t)$. This approach is valid when the contribution of adiabatic noise to spontaneous decay is negligible, a necessary condition being $t \ll T_1^{\text{A}} \propto S_{E_A}(\Omega_\alpha)^{-1}$. This condition is usually satisfied at short enough times, since $S_{E_A}^{1/f}(\omega)$ is substantially different from zero only at frequencies $\omega \ll \Omega_\alpha$. This fact suggests how to trace-out different noise classes in the appropriate order. The total density matrix parametrically depends on the specific realization of the slow random drives $\vec{E}(t)$ and may be written as $\rho^{\text{Q,A,SC}}(t) = \rho^{\text{Q,SC}}(t|\vec{E}(t))$. The first step is to trace out quantum noise. In the simplest cases this requires solving a master equation. In a second stage, the average over all the realizations of the stochastic processes, $\vec{E}(t)$, is performed. This leads to a reduced density matrix for the 2-qubit system plus the strongly coupled degrees of freedom. These latter have to be traced out in a final stage by solving the Heisenberg equations of motion, or by approaches suitable to the specific microscopic Hamiltonian or interaction. For instance, the dynamics may be solved exactly for some special quantum impurity models at pure dephasing, when impurities are longitudinally coupled to each qubit [35, 36]. The multi-stage elimination can be formally written as

$$\rho(t) = Tr_{\text{SC}} \left\{ \int \mathcal{D}[\vec{E}(t)] P[\vec{E}(t)] Tr_{\text{Q}} \left[\rho^{\text{Q,SC}}(t|\vec{E}(t)) \right] \right\}, \quad (10)$$

where Tr_{Q} and Tr_{SC} indicate respectively the trace over the Q and SC degrees of freedom. In the following Sections we apply the multi-stage approach to the two-qubit gate by tracing out first quantum noise and secondly the adiabatic noise. In Appendix B the effect of a SC impurity will be analyzed.

3.1. Relevant dynamical quantities

We focus on the $\sqrt{i - \text{SWAP}}$ operation $|+\rangle - |-\rangle \rightarrow |\psi_e\rangle = [|+\rangle - |-\rangle - i |-\rangle + |+\rangle] / \sqrt{2}$ which generates by free evolution an entangled state at $t_e = \pi/2\omega_c$. As an unambiguous test of entanglement generation and its degradation due to noise, we calculate the evolution of concurrence during the gate operation. Introduced in ref. [28], the concurrence quantifies the entanglement of a pair of qubits, being $C = 0$ for separable states and $C = 1$ for maximally entangled states. For the situations discussed in the present article and specified in the following Sections, the two-qubits RDM takes the "X-form", i.e. the RDM expressed in the eigenstates basis is non-vanishing only along the diagonal and anti-diagonal at any time. Under these conditions, the concurrence can be evaluated in analytic form [37]. In general, it depends both on diagonal and off-diagonal elements of the RDM.

In order to directly compare with experiments where bit-wise readout is performed, we also evaluate the qubit 1 switching probability $P_{\text{SW1}}(t)$, i.e. the probability that it will pass to the state $|-\rangle_1$ starting from the state $|+\rangle_1$; and the probability $P_2(t)$ of finding the qubit 2 in the initial state $|-\rangle_2$. In terms of the two qubit RDM in the eigenstate basis they read ($\text{Tr}_i \rho(t)$ denotes partial trace over qubit i of the two-qubit density matrix)

$$P_{\text{SW1}}(t) = {}_1\langle - | \text{Tr}_2 \rho(t) | - \rangle_1 = \frac{1}{2} [\rho_{11}(t) + \rho_{22}(t)] + \rho_{00}(t) \\ + [\rho_{33}(t) - \rho_{00}(t)] \sin^2 \frac{\varphi}{2} + \text{Re}[\rho_{12}(t)] + \text{Re}[\rho_{03}(t)] \sin \varphi \quad (11)$$

$$P_2(t) = {}_2\langle - | \text{Tr}_1 \rho(t) | - \rangle_2 = \frac{1}{2} [\rho_{11}(t) + \rho_{22}(t)] + \rho_{00}(t) \\ + [\rho_{33}(t) - \rho_{00}(t)] \sin^2 \frac{\varphi}{2} - \text{Re}[\rho_{12}(t)] + \text{Re}[\rho_{03}(t)] \sin \varphi. \quad (12)$$

For preparation in the state $|+ -\rangle$, in the absence of external fluctuations the above probabilities read

$$P_{\text{SW1}}(t) = \frac{1 - \cos \omega_c t}{2}, \quad P_2(t) = \frac{1 + \cos \omega_c t}{2}. \quad (13)$$

The cyclic anti-correlation of the probabilities signals the formation of the entangled state, as reported in various recent experiments [5, 6, 8, 38].

Both the concurrence and the switching probabilities depend on combinations of populations and coherences in the eigenbasis. Therefore the relevant time scale to quantify the "quality factor" or the efficiency of the universal two-qubit gate is not simply related to a specific RDM element, as a difference with a single qubit gate, where the decay time of the qubit coherence quantifies the quality factor of the operation (with T_2 due partly to relaxation processes ($2T_1$), partly to Markovian pure dephasing processes T_2^* or originated from inhomogeneous broadening). In the following we will study the time dependence of coherences and populations, and identify the environmental processes (transverse, longitudinal, low frequency, high frequency, etc.) which originate various decay times. Based on this analysis we will discuss the resulting effect on the decay of the switching probabilities and of the concurrence.

4. Quantum noise

To begin with, we consider the effect of quantum noise replacing in (9) $\hat{E}_\alpha \rightarrow \hat{E}_\alpha^{\text{Q}}$. The system dynamics is obtained by solving the Born-Markov master equation for the RDM. In the system eigenstate basis and performing the secular approximation (to be self-consistently checked) it takes the standard form [39, 40]:

$$\dot{\rho}_{ii}(t) = - \sum_{m \neq i} \Gamma_{im} \rho_{ii}(t) + \sum_{m \neq i} \Gamma_{mi} \rho_{mm}(t) \quad (14)$$

$$\dot{\rho}_{ij}(t) = - (i\tilde{\omega}_{ij} + \tilde{\Gamma}_{ij}) \rho_{ij}(t). \quad (15)$$

The rates Γ_{im} , $\tilde{\Gamma}_{ij}$ and the frequency shifts $\tilde{\omega}_{ij} - \omega_{ij}$, where $\omega_{ij} = \omega_i - \omega_j$, depend respectively on the real and imaginary parts of the lesser and greater Green's functions

which describe emission (absorption) rates to (from) the reservoirs

$$\int_0^\infty dt e^{i\omega t} \langle \langle \hat{E}_\alpha(t) \hat{E}_\alpha(0) \rangle \rangle = \frac{1}{2} C_{E_\alpha}(\omega) - \frac{i}{2} \mathcal{E}_{E_\alpha}(\omega) \quad (16)$$

$$\int_0^\infty dt e^{i\omega t} \langle \langle \hat{E}_\alpha(0) \hat{E}_\alpha(t) \rangle \rangle = \frac{1}{2} C_{E_\alpha}(-\omega) + \frac{i}{2} \mathcal{E}_{E_\alpha}(-\omega). \quad (17)$$

In terms of the corresponding power spectra they read

$$C_{E_\alpha}(\omega) = \frac{2 S_{E_\alpha}(\omega)}{1 + \exp(-\omega/k_B T)} \quad (18)$$

$$\mathcal{E}_{E_\alpha}(\omega) = \mathcal{P} \int_{-\infty}^\infty \frac{d\omega'}{2\pi} \frac{C_{E_\alpha}(\omega')}{\omega' - \omega}, \quad (19)$$

where \mathcal{P} denotes the principal value of the integral. Due to the symmetry of $\mathcal{H}_0 + \mathcal{H}_1$, Eqs. (3) - (4), the only independent emission rates, Γ_{ij} , are $\Gamma_{10} = \Gamma_{32}$, $\Gamma_{20} = \Gamma_{31}$, Γ_{21} , Γ_{30} , see figure 1. Symmetric relations hold between the corresponding absorption rates Γ_{ji} . These processes originate from "effective transverse" noise, in particular transverse fluctuations ($\propto \hat{x}_\alpha$) enter the rates connecting the SWAP and the Z subspaces, whereas longitudinal fluctuations ($\propto \hat{z}_\alpha$) enter the intra-subspace rates, Γ_{21} , Γ_{30} , cfr eqs. (4) - (7). They read

$$\begin{aligned} \Gamma_{10} &= \frac{1}{8} (1 + \sin \varphi) [C_{x_1}(\omega_{10}) + C_{x_2}(\omega_{10})] && \text{inter - subspace} \\ \Gamma_{20} &= \frac{1}{8} (1 - \sin \varphi) [C_{x_1}(\omega_{20}) + C_{x_2}(\omega_{20})] && \text{inter - subspace} \\ \Gamma_{30} &= \frac{1}{4} \sin^2 \varphi [C_{z_1}(\omega_{30}) + C_{z_2}(\omega_{30})] && \text{intra - subspace} \\ \Gamma_{21} &= \frac{1}{4} [C_{z_1}(\omega_{21}) + C_{z_2}(\omega_{21})] && \text{intra - subspace} \end{aligned} \quad (20)$$

Absorption rates have the same form with $C_{E_\alpha}(\omega_{lm})$ replaced by $C_{E_\alpha}(-\omega_{lm})$. The imaginary parts of the corresponding terms take similar forms. They enter the frequency shifts as reported in Appendix C.

In the secular approximation, the SWAP and Z coherences decay exponentially with rates

$$\tilde{\Gamma}_{12} = \frac{1}{2} [\Gamma_{10} + \Gamma_{01} + \Gamma_{20} + \Gamma_{02} + \Gamma_{12} + \Gamma_{21}] \quad (21)$$

$$\tilde{\Gamma}_{30} = \frac{1}{2} [\Gamma_{10} + \Gamma_{01} + \Gamma_{20} + \Gamma_{02} + \Gamma_{30} + \Gamma_{03}] + \Gamma_Z^*, \quad (22)$$

both inter-subspace and intra-subspace rates enter the decay of the SWAP and Z coherences. Note that the decay rate of the coherence $\rho_{12}(t)$ is only originated from dissipative processes (intra- or inter- effective transverse) since no pure dephasing processes (effective longitudinal noise) inside the SWAP subspace exist, cfr eq. (4). On the contrary, the coherences in the Z subspace also decay because of the effective longitudinal terms $\cos \varphi (|0\rangle\langle 0| - |3\rangle\langle 3|)(\hat{z}_1 + \hat{z}_2)$, which originate $\Gamma^{Z*} = \frac{1}{4} \cos^2 \varphi [S_{z_1}(0) + S_{z_2}(0)]$. This pure dephasing factor adds up to a decoherence rate due to intra-subspace effective transverse noise having the characteristic form $[T_2^Z]^{-1} = (\Gamma_{30} + \Gamma_{03})/2$, as implied by (6), and to inter-doublet relaxation rates.

Equations (14) for the populations do not decouple even in the secular limit. General solutions are quite cumbersome, so here we report expressions in the small

temperature limit with respect to the uncoupled qubits splittings, $k_B T \ll \Omega$. In this regime, if the system is initially prepared in the state $|+-\rangle = (|2\rangle - |1\rangle)/\sqrt{2}$, level 3 is not populated, $\rho_{33}(t) = 0$, and the Z-coherences vanish, $\rho_{03}(t) = \rho_{03}(0) = 0$. The remaining populations are conveniently expressed in terms of the escape rates from levels 1 and 2

$$\Gamma_1^e = \Gamma_{10} + \Gamma_{12} \quad , \quad \Gamma_2^e = \Gamma_{20} + \Gamma_{21} \quad , \quad (23)$$

which enter the evolution of the populations in the following combinations

$$\Gamma_{\pm} = \frac{\Gamma_1^e + \Gamma_2^e}{2} \mp \frac{1}{2} \sqrt{(\Gamma_1^e - \Gamma_2^e)^2 + 4\Gamma_{12}\Gamma_{21}} \quad . \quad (24)$$

For the chosen initial conditions the populations read

$$\rho_{11}(t) = \frac{\Gamma_{21}}{2(\Gamma_- - \Gamma_+)} \sum_{k=\pm} k \left[1 + \frac{\Gamma_{12}}{\Gamma_1^e - \Gamma_k} \right] e^{-\Gamma_k t} \quad (25)$$

$$\rho_{22}(t) = \frac{1}{2(\Gamma_- - \Gamma_+)} \sum_{k=\pm} k [\Gamma_{12} - \Gamma_k + \Gamma_1^e] e^{-\Gamma_k t} \quad (26)$$

$$\rho_{00}(t) = 1 - (\rho_{11}(t) + \rho_{22}(t)) \quad . \quad (27)$$

Note that, since $k_B T \lesssim \omega_c \ll \Omega$, thermal excitation processes internal to the SWAP subspace, expressed via the absorption rate Γ_{12} , cannot be neglected and $\Gamma_{21} \approx \Gamma_{12}$. On the contrary, inter-doublet thermal excitation processes are exponentially suppressed with respect to the corresponding decay rates, $\Gamma_{01}, \Gamma_{02} \ll \Gamma_{10}, \Gamma_{20}$, with $\Gamma_{10} \approx \Gamma_{20}$. Thus the SWAP coherences decay rate (21) is approximately half the sum of the escape rates (23)

$$\tilde{\Gamma}_{12} \approx \frac{\Gamma_1^e + \Gamma_2^e}{2} \quad . \quad (28)$$

In order to observe generation of entanglement inside the SWAP subspace it is necessary that relaxation processes to the ground state take place on a sufficiently long time scale. This is guaranteed when inter- and intra-subspace rates satisfy the condition $\Gamma_{10}, \Gamma_{20} \ll \Gamma_{21}, \Gamma_{12}$, which requires that the spectra of the originally transverse and longitudinal fluctuations are $S_{x_\alpha}(\Omega) \ll S_{z_\alpha}(\omega_c)$ (from (20)). In this regime, the SWAP decoherence rate (28) is due to effective transverse processes internal to the subspace

$$\tilde{\Gamma}_{12} \approx \frac{1}{2} [\Gamma_{12} + \Gamma_{21}] \quad , \quad (29)$$

and the scales entering the populations take the approximate forms

$$\Gamma_+ \approx \frac{1}{2} [\Gamma_{10} + \Gamma_{20}] \quad \text{relaxation to the ground state} \quad (30)$$

$$\Gamma_- \approx \Gamma_{12} + \Gamma_{21} \quad \text{relaxation inside the SWAP subspace} \quad (31)$$

with $\Gamma_+ \ll \Gamma_-$. Therefore, the time scales resulting from quantum noise, considering that $k_B T \lesssim \omega_c \ll \Omega$, when $S_{x_\alpha}(\Omega) \ll S_{z_\alpha}(\omega_c)$, are

- "Global" relaxation time to the ground state, analogous to the single qubit T_1 : Its order of magnitude is the spectrum of *transverse fluctuations* in the computational basis at frequency Ω

$$T_R = 1/\Gamma_+ \approx \frac{8}{C_{x_1}(\Omega) + C_{x_2}(\Omega)} = \frac{4}{S_{x_1}(\Omega) + S_{x_2}(\Omega)}, \quad (32)$$

where the approximate form comes from eq. (20), where $\omega_{10} \approx \omega_{20} \approx \Omega$.

- Relaxation/decoherence times inside the SWAP subspace: They are due to "effective transverse" fluctuations inside this subspace, physically originated from *longitudinal noise* on each qubit at frequency ω_c . Since there is no effective longitudinal noise in the SWAP subspace, relaxation and dephasing times are related by the typical relation $T_2^{SWAP} \approx 2T_1^{SWAP}$ where

$$T_1^{SWAP} = 1/\Gamma_- \approx 1/(2\tilde{\Gamma}_{12}) \quad (33)$$

$$T_2^{SWAP} = 1/\tilde{\Gamma}_{12} \approx \frac{4}{S_{z_1}(\omega_c) + S_{z_2}(\omega_c)}. \quad (34)$$

We now briefly comment on the validity of the secular approximation. It consists in separating the evolutions of elements $\rho_{ij}(t)$ and $\rho_{lm}(t)$ provided that $|\omega_{ij} - \omega_{lm}| \gg \tau^{-1}$, where τ denotes the typical evolution time scale of the system [39]. In the present case this condition is fulfilled if $\omega_{21} \approx \omega_c \gg \tilde{\Gamma}_{12}$. This constraint, on the other side, *needs* to be satisfied in order to observe generation of entanglement in the presence of quantum noise, as expressed for instance from anti-correlation of the probabilities (11) and (12). Thus it can be regarded as a *necessary condition*, whose validity has to be checked case by case and requires (from (21))

$$S_{x_\alpha}(\Omega), S_{z_\alpha}(\omega_c) \ll \omega_c. \quad (35)$$

In conclusion, entanglement generation in the presence of transverse and longitudinal quantum noise is guaranteed when

$$S_{x_\alpha}(\Omega) \ll S_{z_\alpha}(\omega_c) \quad (36)$$

$$\tilde{\Gamma}_{12} \approx \frac{S_{z_1}(\omega_c) + S_{z_2}(\omega_c)}{4} \ll \omega_c. \quad (37)$$

Under these conditions, the "global" relaxation time and the SWAP relaxation and decoherence times are given respectively by eqs. (32) and (33), (34). We note that, as a limiting case, the \sqrt{i} -SWAP operation can be realized also releasing the condition $\Gamma_+ \ll \Gamma_-$, provided both rates are much smaller than the coupling strength ω_c , and $\tilde{\Gamma}_{12} \ll \omega_c$. For instance, when $(\omega_c/\Omega)S_{x_\alpha}(\Omega) \ll S_{z_\alpha}(\omega_c) \ll \omega_c$ in Eq. (24) $|\Gamma_{10} - \Gamma_{20}| \ll \Gamma_{21} + \Gamma_{12}$ and the rates Γ_\pm are still given by Eqs. (30), (31) leading to $T_R = 1/\Gamma_+$ and $T_1^{SWAP} = 1/\Gamma_-$. The SWAP dephasing time in this case also depends on trasverse fluctuations, $T_2^{SWAP} = 1/\tilde{\Gamma}_{21} \approx 1/[\Gamma_+ + \Gamma_-/2]$.

Table 3. Noise characteristics deduced from single qubit data reported in ref.[3]. Since both qubits operate at $q_{\alpha,x} = 1/2$, they are presumably affected by similar polarization fluctuations, thus σ_{x_α} and S_{x_α} are the same as in table 2. Since the two qubits operate at different phase points, their phase spectral characteristics differ. From ref.[3] the power spectrum of phase fluctuations is $S_\delta(\omega) \approx [5.57 \times 10^{-7}]/\omega + 3.7 \times 10^{-14}$ [s] where the extrapolated crossover frequency is $\approx 2\pi 10$ MHz. Since $\delta_2 \neq 0$ the process $\hat{z}_2 \propto \Delta\delta_2$ is Gaussian and characterized by $S_{z_2}(\omega) = (E_{J,2}^0 \sin \delta_2)^2 (\tilde{\Phi}_{2,++} - \tilde{\Phi}_{2,-,-})^2 S_{\delta_2}(\omega)$ (where $\tilde{\Phi}_{2,\pm\pm}$ are defined in Appendix A, table A2). Instead $z_1 \propto (\Delta\delta_1)^2$ is non Gaussian and its spectrum is ohmic, $S_{z_1}(\omega) = 2S^2/(\pi\Omega^2)\omega \coth(\omega/(2K_B T))$, where $S = 1.6 \times 10^8 \text{s}^{-1}$. In this table we fixed $\Omega \approx 10^{11} \text{rad/s}$, $\omega_c \approx 10^{-2}\Omega$ and $T = 40$ mK.

	Qubit 1	Qubit 2
$S_x^{1/f}$	$\sigma_{x_1} \approx 2 \times 10^{-2} \Omega$	$\sigma_{x_2} \approx 2 \times 10^{-2} \Omega$
$S_z^{1/f}$	$\sigma_{z_1} \approx 10^{-6} \Omega$	$\sigma_{z_2} \approx 6 \times 10^{-4} \Omega$
S_x^f	$S_{x_i}(\Omega) \approx 4 \times 10^6 \text{s}^{-1}$	$S_{x_i}(\Omega) \approx 4 \times 10^6 \text{s}^{-1}$
S_z^f	$S_{z_1}(\omega_c) \approx 10^4 \text{s}^{-1}$	$S_{z_2}(\omega_c) \approx 5 \times 10^7 \text{s}^{-1}$

4.1. Switching probabilities

In the secular approximation, for preparation at $t = 0$ in $|+ - \rangle$ and for $k_B T \ll \Omega$, the probabilities (11) and (12) take the simpler form

$$P_{\text{SW1}}(t) = -\frac{1}{2} \cos \varphi [\rho_{11}(t) + \rho_{22}(t)] + \text{Re}[\rho_{12}(t)] + \cos^2 \left(\frac{\varphi}{2} \right) \quad (38)$$

$$P_2(t) = -\frac{1}{2} \cos \varphi [\rho_{11}(t) + \rho_{22}(t)] - \text{Re}[\rho_{12}(t)] + \cos^2 \left(\frac{\varphi}{2} \right). \quad (39)$$

where $\rho_{11}(t)$ and $\rho_{22}(t)$ are given by eqs. (25), (26) and

$$\rho_{12}(t) = \rho_{12}(0) \exp \{ -t/T_2^{\text{SWAP}} - i\tilde{\omega}_{12}t \}.$$

Anti-correlation of the above probabilities directly follows from the coherence $\rho_{12}(t)$ entering with different signs in $P_{\text{SW1}}(t)$ and in $P_2(t)$. In order to check the efficiency of the gate we will therefore consider only the qubit 1 switching probability. Neglecting the frequency shift of ω_{21} (see Appendix C), $P_{\text{SW1}}(t)$ can be approximated as

$$P_{\text{SW1}}(t) \approx \frac{1}{2} [e^{-t/T_R} - \cos(\omega_{21}t) e^{-t/T_2^{\text{SWAP}}}] + \cos^2 \left(\frac{\varphi}{2} \right). \quad (40)$$

Here we explicitly see that, in order to perform the $\sqrt{i - \text{SWAP}}$ operation, it is necessary that $T_R, T_2^{\text{SWAP}} \gg 1/\omega_c$. Efficient entanglement generation is guaranteed when $T_R \gg T_2^{\text{SWAP}} \gg 1/\omega_c$, i.e. when transverse and longitudinal quantum noise are such that $S_{x_\alpha}(\Omega) \ll S_{z_\alpha}(\omega_c)$. Under this condition, the efficiency of the gate is limited by T_2^{SWAP} , i. e. by longitudinal noise in the computational basis, $S_{z_\alpha}(\omega_c)$, which is responsible for the short-times behavior. Decay towards the equilibrium value $P_{\text{SW1}}(\infty) = \cos^2(\varphi/2) = (1 + \cos \varphi)/2 = (1 - 1/\sqrt{1 + (\omega_c/2\Omega)^2})/2 \approx (\omega_c/4\Omega)^2$ occurs in a time of the order of T_R , due to transverse noise in the computational basis.

Capacitively coupled CPB-based qubits: The relevant rates (20) can be estimated in this specific case and are reported in Appendix A. For the charge-phase two-ports

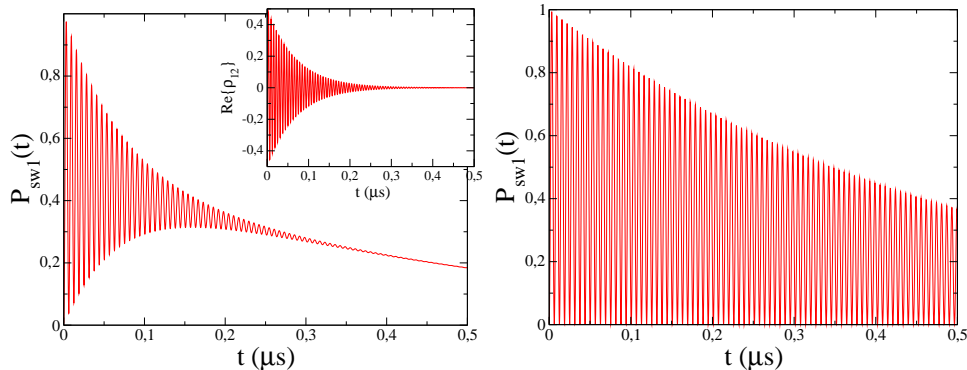


Figure 3. Left panel: Switching probability of qubit 1 for the noise levels S_x^f and S_z^f reported in table 3. The long-time decay is due to charge noise entering the populations of levels 1 and 2. Inset: the real part of the SWAP coherence which is responsible for the short-time behavior of the switching probability due to phase noise on qubit 2. Right panel: Switching probability of qubit 1 in the presence of charge noise with white spectrum, $S_{x_i}(\omega) \approx 4 \times 10^6 \text{s}^{-1}$.

architecture, control is via the gate voltage, $q_x = C_g V_g / (2e)$ and magnetic flux dependent phase, δ , entering the Josephson energy. The single qubit optimal point is at $q_x = 1/2$, $\delta = 0$. The resonant condition between the two qubits with a capacitive coupling is achieved by displacing one of the two qubits from the "double" optimal point. In order to limit the sensitivity to charge noise, resonance is achieved tuning $\delta_2 \approx 0.45$. The noise characteristics are reported in table 3, where we note that $S_{x_\alpha}(\Omega) \ll S_{z_\alpha}(\omega_c)$. Because of the operating conditions, absorption (and emission) rates due to phase noise on qubit 2 dominate over rates due both to charge noise and to phase noise on qubit 1. Relaxation of the populations takes place on a scale $1/T_R = \Gamma_+ \approx \Gamma_{10} \approx \Gamma_{20} \approx S_{x_i}(\Omega)/2$ due to transverse (charge) noise on both qubits, whereas the SWAP coherence decay rate is dominated by longitudinal (phase) noise on qubit 2, $1/T_2^{SWAP} = \tilde{\Gamma}_{12} \approx \frac{1}{2}(\Gamma_{12} + \Gamma_{21}) \approx \Gamma_{21} \approx S_{z_2}(\omega_c)/4$. The efficiency of the $\sqrt{i - \text{SWAP}}$ gate is mainly limited by phase noise on qubit 2, which gives $T_2^{SWAP} \approx 1/\Gamma_{21} \approx 100$ ns. We note that, under these conditions, T_2^{SWAP} is comparable with the decoherence time of qubit 2, $T_2 = 1/[S_{x_2}(\Omega)/4 + S_{z_2}(0)/2] \approx 2/S_{z_2}(0) \approx 2/S_{z_2}(\omega_c)$. The phase-dominated behavior is followed by a slower charge-dominated decay towards the equilibrium value $P_{SW1}(\infty) \approx (\omega_c/4\Omega)^2$. These features are illustrated in figure 3 (left) where for comparison the real part of the SWAP coherence is shown in the inset. We note that the contribution of high-frequency charge noise to the efficiency of the $\sqrt{i - \text{SWAP}}$ gate is relatively small. Indeed if only polarization fluctuations were present, we could approximate

$$P_{SW1}(t) \approx \frac{1}{2} [1 - \cos(\omega_{21}t)] e^{-t/T_2^{SWAP}} + \cos^2\left(\frac{\varphi}{2}\right) \quad (41)$$

and $T_2^{SWAP} \approx 1/\Gamma_{10} \approx 0.5 \mu\text{s}$. This situation is illustrated in figure 3 (right). Note that for the estimated noise figures, the condition for the secular approximation, $\omega_{21} = \omega_c \gg \tilde{\Gamma}_{12}$, is satisfied.

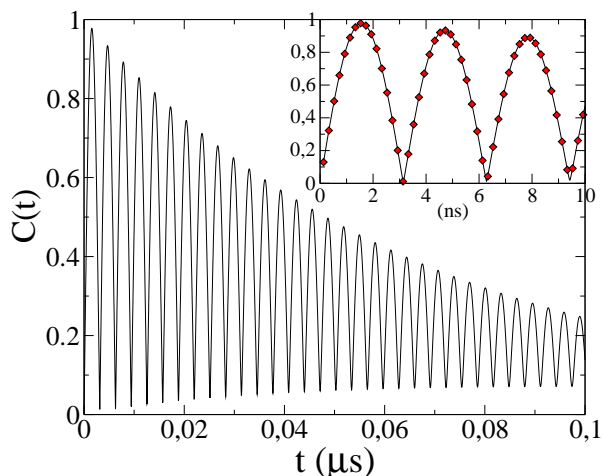


Figure 4. Concurrence given by (43) for $\omega_c/\Omega = 0.01$ and for quantum noise values S_x^f and S_z^f reported in table 3. Inset: At short times $C(t) \approx 2|\text{Im}\{\rho_{12}(t)\}|$ (diamonds).

4.2. Concurrence

For the considered initial condition, the RDM takes the "X-form" [37] and the concurrence is given by

$$C(t) \approx \max \left[0, \sqrt{(\rho_{11}(t) - \rho_{22}(t))^2 + (2\text{Im}[\rho_{12}(t)])^2} - |\sin \varphi| \rho_{00}(t), \right. \\ \left. |\sin \varphi| \rho_{00}(t) - \sqrt{(\rho_{11}(t) + \rho_{22}(t))^2 - (2\text{Re}[\rho_{12}(t)])^2} \right]. \quad (42)$$

At times shorter than the global relaxation time, T_R , the ground state is almost unpopulated, $\rho_{00}(t) \approx 0$, and $C(t)$ is given by the second term in (42)

$$C(t) \approx \left[\frac{\Gamma_+}{\Gamma_-} e^{-2t/T_R} + \sin^2(\omega_{12}t) e^{-2t/T_2^{SWAP}} \right]^{1/2} - |\sin \varphi| (1 - e^{-t/T_R}), \quad (43)$$

for $t \ll T_R$, the concurrence is approximately given by the SWAP coherence $C(t) \approx 2|\text{Im}\{\rho_{12}(t)\}| = \sin(\omega_{12}t) e^{-t/T_2^{SWAP}}$. Like the switching probabilities, the concurrence evolves with the SWAP coherence decay time, T_2^{SWAP} , due to originally longitudinal noise.

Capacitively coupled CPB-based qubits: The concurrence for the charge-phase 2-qubit gate is illustrated in figure 4. We note that the long-time behavior is instead due to populations relaxation to the ground state and $C(t)$ is given by the third term in (42)

$$C(t) \approx |\sin \varphi| (1 - e^{-t/T_R}) - \left[e^{-2t/T_R} - \cos^2(\omega_{12}t) e^{-2t/T_2^{SWAP}} \right]^{1/2} \\ \approx -|\sin \varphi| \rho_{00}(t) \rightarrow |\sin \varphi| \quad (44)$$

The finite asymptotic value $C(t \rightarrow \infty) \approx |\sin \varphi|$, reflects the entangled thermalized state. Because of the interaction between the two qubits the phenomenon of entanglement sudden death does not take place [37].

5. Adiabatic noise

Let's consider now the effect of low frequency fluctuations, replacing in (9) $\hat{E}_\alpha \rightarrow \hat{E}_\alpha^A \equiv E_\alpha(t)$. In the adiabatic and longitudinal approximation [22, 34] populations do not evolve and the system dynamics is related to instantaneous eigenvalues, $\omega_i(\vec{E}(t))$, which depend on the noise realization, $\vec{E}(t)$. They enter the coherences in the eigenbasis of \mathcal{H}_0 in the form

$$\rho_{ij}(t) = \rho_{ij}(0) \int \mathcal{D}[\vec{E}(s)] P[\vec{E}(s)] e^{-i \int_0^t ds \omega_{ij}(\vec{E}(s))} \quad (45)$$

where the probability of the realization $\vec{E}(s)$, $P[\vec{E}(s)]$, also depends on the measurement protocol. A standard approximation of the path-integral (45) consists in replacing $E_\alpha(t)$ with statistically distributed values $E_\alpha(0) \equiv E_\alpha$ at each repetition of the measurement protocol. The "static-path approximation" (SPA) [22] or "static-noise" approximation [13] gives the leading order effect of low-frequency fluctuations in repeated measurements. In the SPA, the level splittings $\omega_{ij}(\vec{E})$ are random variables, with standard deviation $\Sigma_{ij} = \sqrt{\langle \delta\omega_{ij}^2 \rangle - \langle \delta\omega_{ij} \rangle^2}$, where $\delta\omega_{ij} = \omega_{ij}(\vec{E}) - \omega_{ij}$. The coherences (45) reduce to ordinary integrals

$$\rho_{ij}(t) \approx \rho_{ij}(0) \int d\vec{E} P(\vec{E}) e^{-i\omega_{ij}(\vec{E})t} \equiv \rho_{ij}(0) \langle e^{-i\omega_{ij}(\vec{E})t} \rangle, \quad (46)$$

where the probability density, in relevant cases, can be taken of Gaussian form, $P(\vec{E}) \equiv \Pi_\alpha P(E_\alpha)$ with $P(E_\alpha) = \exp[-E_\alpha^2/2\sigma_{E_\alpha}^2]/\sqrt{2\pi}\sigma_{E_\alpha}$ [22]. The splittings $\omega_{ij}(\vec{E})$ come both from "effective longitudinal" and from "effective transverse" terms in (4). This is analogous to a single qubit, where longitudinal noise gives the leading order linear terms and transverse noise is responsible for second order terms which dominate at the optimal point, where the first order longitudinal contributions vanish [13, 44]. Here, the Z-splitting $\omega_{03}(\vec{E})$ has a linear contribution due to the effective longitudinal noise $(\hat{z}_1 + \hat{z}_2) \cos \varphi (|0\rangle\langle 0| - |3\rangle\langle 3|)$ in (6). The SWAP splitting $\omega_{21}(\vec{E})$ instead, in the absence of leading-order effective-longitudinal intra-doublet terms in (5), comes from higher order contributions due to "effective transverse" noise. Evaluating them requires considering the complete Hilbert space of the coupled qubit system (inter-doublet processes included). The systematic approach to obtain these contributions consists in treating in perturbation theory effective transverse terms in \mathcal{H}_I , where, in the adiabatic approximation, \hat{x}_α and \hat{z}_α are replaced by classical stochastic fields x_α and z_α . We obtain

$$\begin{aligned} \omega_{21}(x_1, x_2, z_1, z_2) \approx & \omega_c - \frac{\omega_c}{2\Omega^2}(x_1^2 + x_2^2) + \frac{1}{2\omega_c}(z_1 - z_2)^2 \\ & + \frac{\omega_c}{2\Omega^3}(x_1^2 + x_2^2)(z_1 + z_2) + \frac{1}{2\omega_c\Omega}(x_1^2 - x_2^2)(z_1 - z_2) \\ & + \frac{\omega_c}{8\Omega^4}\left(1 + \frac{\omega_c^2}{\Omega^2}\right)(x_1^4 + 6x_1^2x_2^2 + x_2^4) + \frac{1}{8\omega_c\Omega^2}(x_1^2 - x_2^2)^2, \end{aligned} \quad (47)$$

$$\begin{aligned} \omega_{03}(x_1, x_2, z_1, z_2) &\approx 2\sqrt{\frac{\omega_c^2}{4} + \Omega^2} - \cos \varphi (z_1 + z_2) \\ &+ \frac{1}{2\Omega} \left(\frac{\omega_c}{\Omega} \sin \varphi - \cos \varphi \right) (x_1^2 + x_2^2) + \frac{\omega_c}{8\Omega^2} \sin \varphi (z_1 + z_2)^2, \end{aligned} \quad (48)$$

where $\tan \varphi = -\omega_c/(2\Omega)$. The SWAP-splitting has been evaluated up to 4th order [41], whereas the Z splitting expansion is considered up to second order since the fourth-order terms are much smaller, scaling with ω_c^3 . The Z-splitting consists of a linear term due to the effective longitudinal noise, which dominates with respect to the quadratic term due to effective transverse intra-subspace noise (scaling with $\sin \varphi$). Transverse inter-doublet noise gives an additional second order contribution.

Performing the average (46) (including in the 3rd and 4th order terms in (47) only the contributions $\propto \omega_c^{-1}$) we obtain the SWAP coherence in the SPA

$$\rho_{12}^{SPA}(t) = \rho_{12}(0) \frac{\Omega}{2\sigma_x^2} \sqrt{\frac{2i\omega_c}{\pi t}} e^{i\omega_c t + h(t)} K_0[h(t)] \quad (49)$$

where $h(t) = (\sigma_{z_1}^2 + \sigma_{z_2}^2 + i\omega_c/t) (\Omega^2/\sigma_x^2 + i\omega_c t)^2/(4\Omega^2)$ and $K_0[h]$ is the K-Bessel function of order zero [42]. In the absence of mixed terms in the expansion (48), different contributions to the Z-coherence factorize and lead to

$$\rho_{03}^{SPA}(t) = \rho_{03}(0) e^{2i\sqrt{\frac{\omega_c^2}{4} + \Omega^2} t} \frac{e^{-\frac{|\cos \varphi|}{2} (\sigma_{z_1}^2 + \sigma_{z_2}^2) t^2}}{1 - \frac{i}{\Omega} \left(\frac{\omega_c}{\Omega} \sin \varphi - \cos \varphi \right) \sigma_x^2 t}. \quad (50)$$

Here we assumed the same variance for the transverse noise components, $\sigma_{x_1} = \sigma_{x_2} \equiv \sigma_x$. Instead we maintained σ_{z_1} and σ_{z_2} distinct, considering that the two qubits may operate at different working points (Appendix A). In (50) the exponential factor comes from linear terms in (48) due to effective longitudinal noise in the Z-subspace. The algebraic decay instead comes from quadratic terms in the expansion of ω_{03} , due to effective transverse inter-doublet processes.

We remark that the applicability of the Gaussian approximation to the fields E_α depends on the relation between each E_α and the fluctuations of the system's physical parameters. For instance, for a charge-phase $\sqrt{i} - \text{SWAP}$ gate the resonant condition occurs for $\delta_1 = 0$, $\delta_2 \neq 0$ (Appendix A). Thus it is $z_1 \propto E_{1,J}^0 (\Delta\delta_1)^2$, where δ_1 (not z_1) is reasonably assumed Gaussian distributed. This would result in a modification of the terms $\propto \sigma_{z_1}$ in Eqs. (49) and (50). For instance, the integral over z_1 in ρ_{03}^{SPA} would reduce to $\{1 - i\sqrt{2} \cos \varphi \sigma_{z_1} t\}^{-1/2}$, instead of $\exp\{-|\cos \varphi| \sigma_{z_1}^2 t^2/2\}$. The quantitative effect in $\rho_{03}^{SPA}(t)$ (and similarly in $\rho_{12}^{SPA}(t)$) is however negligible, because of the smallness of longitudinal noise at the optimal point, $\sigma_{z_1} \ll \sigma_{z_2}$ (see table 3).

Validity regime of the SPA: The adiabatic approximation is tenable for times shorter than the relaxation times, for this problem this condition requires that $t \ll T_1^{SWAP}$. The static approximation is exact for times smaller than $1/\gamma_M$ (in case of a sharp high frequency cut-off). We verified that it is a good approximation also for times $t > 1/\gamma_M$ if $\gamma_M < \Omega$ and the $1/f$ spectrum is originated from an ensemble of bistable fluctuators with switching rates $\in [\gamma_m, \gamma_M]$, leading to a $1/f^2$ decay above γ_M (numerical simulations and analytic first correction to the SPA [22]).

5.1. Minimization of defocusing: optimal coupling

Exploiting the band structure of coupled nano-devices it is possible to reduce the influence of $1/f$ fluctuations [43]. The basic idea of "optimal tuning" is to fix control parameters to values which minimize the variance of the splittings $\omega_{ij}(\vec{E})$, Σ_{ij}^2 . This naturally results in an enhancement of the decay time of the corresponding coherence due to inhomogeneous broadening, i. e. of $\rho_{ij}^{SPA}(t)$. This is simply understood considering the short times expansion of $\langle \exp \{-i\delta\omega_{ij}(\vec{E})t\} \rangle$

$$\langle e^{-i\delta\omega_{ij}(\vec{E})t} \rangle \approx 1 - i\langle \delta\omega_{ij}(\vec{E}) \rangle t - \frac{1}{2}\langle \delta\omega_{ij}(\vec{E})^2 \rangle t^2 \quad (51)$$

the short-times decay of the coherence in the SPA is therefore given by

$$|\langle e^{-i\delta\omega_{ij}(\vec{E})t} \rangle| \approx \sqrt{1 - (\Sigma_{ij}t)^2}, \quad (52)$$

resulting in reduced defocusing for minimal variance Σ_{ij} . For a single-qubit gate, the "optimal tuning" idea immediately leads to the well-known "magic point". In fact, if $\omega_{ij}(\vec{E})$ is monotonic in a region $|E_\alpha| \leq 3\sigma_{E_\alpha}$, we can approximate $\Sigma_{ij}^2 \approx \sum_\alpha \left[\frac{\partial \omega_{ij}}{\partial E_\alpha} \Big|_{E_\alpha=0} \right]^2 \sigma_{E_\alpha}^2$, thus the variance attains a minimum for vanishing differential dispersion. For the charge-phase two-port architecture, control is via gate voltage, q_x , and magnetic-flux dependent phase δ , thus E_α corresponds to the fluctuations $\Delta q_x, \Delta E_J$ and the optimal point, $q_x = 1/2, \delta = 0$, is at the a saddle point of the energy bands [3]. When bands are non-monotonic in the control parameters, minimization of defocusing necessarily requires their tuning to values depending on the noise variances. For a multi-qubit gate, the optimal choice has to be done considering the most relevant coherence for the considered operation. Here we show how this program applies to the coherence in the SWAP subspace and partly to $\rho_{03}^{SPA}(t)$.

A key feature is that the SWAP splitting, ω_{21} in Eq. (47) is non-monotonic in the small coupling $\omega_c \ll \Omega$. This is due to the fact that effective transverse fluctuations originate both from longitudinal and transverse noise, and give rise respectively to intra-SWAP and inter-doublet transitions, see (5), (7). For instance, second order corrections to ω_1 from effective transverse intra-doublet processes are $\omega_c^{-1} \propto |\langle 1|\mathcal{H}_I|2 \rangle|^2 / (\omega_1 - \omega_2)$, from effective transverse inter-doublet transitions are $\sum_{i \neq 1,2} |\langle 1|\mathcal{H}_I|i \rangle|^2 / (\omega_1 - \omega_i) \propto \omega_c$.

Non-monotonicity in ω_c results in a competition between 2nd and 4th order x_α -terms in (47) and in non-monotonic band structure, figure 5 (panels (a) and (b)). Because of this subtle feature, identification of the best operating condition necessarily requires consideration of the noise characteristics. Indeed the *optimal coupling* which minimizes the SWAP variance

$$\Sigma_{21}^2 \approx \frac{1}{\omega_c^2} \left\{ \left(\frac{\sigma_x}{\Omega} \right)^4 [(\sigma_x^2 - \omega_c^2)^2 + \sigma_x^4 + \sigma_{z_2}^2 \Omega^2] + \frac{\sigma_{z_2}^4}{2} \right\} \quad (53)$$

is given by

$$\tilde{\omega}_c = \left\{ 2\sigma_x^4 + \sigma_{z_2}^2 \Omega^2 + \frac{1}{2} \left(\frac{\sigma_{z_2} \Omega}{\sigma_x} \right)^4 \right\}^{1/4}, \quad (54)$$

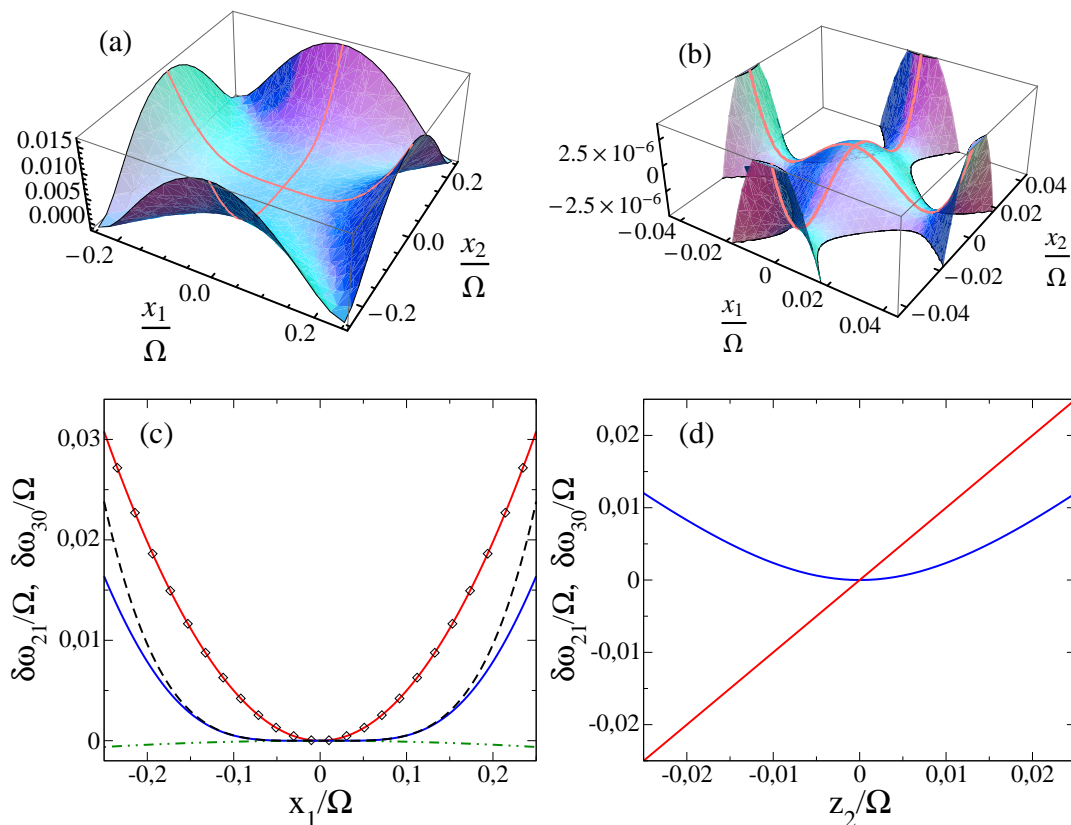


Figure 5. Dispersion of the SWAP and Z splittings for $\omega_c/\Omega = 0.02$. Panels (a) and (b): $\delta\omega_{21}/\Omega$ from numerical diagonalization of $\mathcal{H}_0 + \mathcal{H}_I$. In panel (b) a zoom around the origin highlights the interplay of 2^{nd} and 4^{th} order terms of the expansion (47), the barrier height is $\propto \omega_c^3$. Panel (c): SWAP exact splitting (blue), expansion (47) for $x_2 = 0, z_i = 0$ (dashed), 2^{nd} order expansion (dash-dotted green), Z splitting (red) from (48) and single qubit dispersion (diamonds). Panel (d): Longitudinal dispersions in the SWAP (blue) and Z (red) subspaces.

where we assumed $\sigma_{z_1} \ll \sigma_{z_2}$. The effectiveness of the optimal coupling choice has been discussed in details in ref. [43]. The advantage of operating at optimal coupling with respect to a generic ω_c can be parametrized by the error of the gate at time $t_e = \pi/2\omega_c$ when system should be in the entangled state $|\psi_e\rangle = [|+-\rangle - i|-+\rangle]/\sqrt{2}$, $\varepsilon = 1 - \langle\psi_e|\rho(t_e)|\psi_e\rangle$. As shown in table 4 for two CPB-qubits, in the presence of moderate amplitude transverse (charge) noise, at the optimal coupling the error can be reduced even one order of magnitude with respect to a generic coupling.

The splitting in the Z-subspace, on the contrary, is monotonic both in x_α and in z_α , similarly to a single qubit operating at $q_{\alpha,x} = 1/2$ and at the two different δ_α , figure 5, panels (c) and (d). The most relevant contribution to Z-variance is given by the effective longitudinal noise

$$\Sigma_{03}^2 \approx \cos^2 \varphi \sigma_{z_2}^2, \quad (55)$$

Table 4. Error at the first \sqrt{i} -SWAP operation at time t_e for various couplings ω_c/Ω (numerical simulation of the coupled dynamics). The error ε_a refers to a typical amplitude $\sigma_x = 0.02\Omega$; the error ε_b refers instead to a moderate amplitude $\sigma_x = 0.04\Omega$. Longitudinal noise is here $\sigma_{z_2} = 10^{-3}\Omega$. The optimal coupling, (54), is in both cases at $\tilde{\omega}_c \approx 0.05\Omega$. The error ε_a is reduced by increasing ω_c because of the comparatively large effect of phase noise. In the case of ε_b , the most detrimental effect is from charge noise and the error is minimum at $\tilde{\omega}_c$.

ω_c/Ω	ε_a	ε_b
0.01	$3 \cdot 10^{-3}$	10^{-2}
0.02	$1.5 \cdot 10^{-3}$	$5 \cdot 10^{-3}$
0.04	$6 \cdot 10^{-4}$	$2 \cdot 10^{-3}$
0.05	$8 \cdot 10^{-4}$	$8 \cdot 10^{-4}$
0.06	$3 \cdot 10^{-4}$	10^{-3}
0.08	$2 \cdot 10^{-4}$	$9 \cdot 10^{-4}$

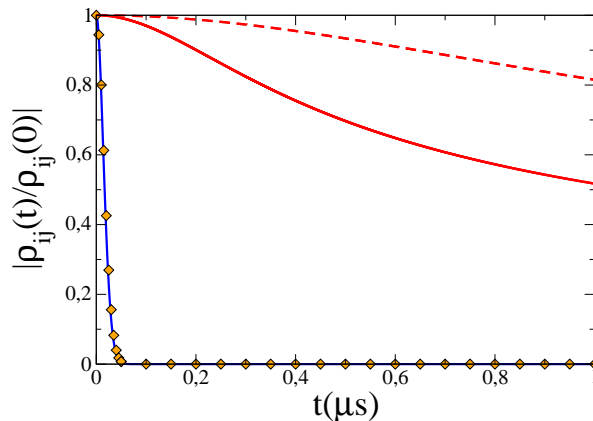


Figure 6. Coherence in the SWAP-subspace (continuous red), in the Z-subspace (blue) and the single qubit-coherence (orange diamonds) for generic coupling $\omega_c = 0.01\Omega$. The dashed red line is the coherence in the SWAP-subspace for optimal coupling, $\tilde{\omega}_c \approx 0.03\Omega$. The Z coherence does not appreciably change by changing ω_c and decays similarly to a single qubit at the double optimal point. Noise characteristics are reported in table 3.

which can be reduced only by increasing the qubit's coupling strength ω_c , which is however limited by single qubit splittings Ω . Therefore, no special optimal point exists if the two-qubit operation involves the dynamics inside the Z-subspace. A comparison of the evolution of the coherences in the two subspaces and of the single qubit-coherence is shown in figure 6 for two CPB-based qubits. In order to keep the advantage of optimal tuning in the SWAP-subspace, the two-qubit operation should not involve the Z-subspace.

Finally, we remark that the above results only follow considering the 4-level spectrum of the coupled devices. In fact, because of mixing between subspaces, limiting the analysis to noise projections inside the subspaces would miss a relevant part of the defocusing processes coming from originally transverse fluctuations $\propto x_\alpha$, see eqs. (3),

(4). This is clear if we consider the evolution of the SWAP coherences truncating the system Hilbert space to the SWAP subspace. Since the reduced Hamiltonian is (5), effective transverse intra-doublet noise would lead to quadratic corrections to the SWAP-splitting \parallel . In fact, treating in perturbation theory z_α up to second order, we would get $\omega_{21}(x_1, x_2, z_1, z_2) \approx \omega_c + \frac{1}{2\omega_c}(z_1 - z_2)^2$ and the SWAP coherence would decay algebraically, as it is typically originated from "effective transverse" low frequency noise

$$\rho_{12}(t) \propto \frac{1}{\sqrt{1 - i(\sigma_{z_1}^2 + \sigma_{z_2}^2)t/\omega_c}}. \quad (56)$$

Under this approximation, reduction of defocusing could only be achieved by increasing the coupling strength. Similarly, reducing the analysis to the Z-subspace, cfr eq. (6), would miss the quadratic dependence of the Z-splitting due to transverse noise.

6. Time scales of the \sqrt{i} -SWAP operation: interplay of quantum and adiabatic noise

In the multi-stage elimination approach, where quantum noise is traced out first and adiabatic noise is retained as a classical stochastic drive, we have to replace in eqs. (25) - (27) and in $\rho_{12}(t) = \rho_{12}(0) \exp\{-t/T_2^{SWAP} - i\tilde{\omega}_{12}t\}$, ω_{ij} with $\omega_{ij}(\vec{E}(t))$ and perform the path-integral over the realizations of $\vec{E}(t)$. Note that the dependence on adiabatic noise enters also the rates, which should be averaged. If the dependence of the power spectra on the splittings is sufficiently smooth, it can be neglected and the effect of low frequency noise reduces to averaging phase factors in the coherences \blacklozenge . Thus, provided that the dependence on \vec{E} of $\tilde{\Gamma}_{21}$ and $\tilde{\Gamma}_{30}$ can be neglected, the effects of quantum and adiabatic noise can be treated independently and lead to

$$\rho_{12}(t) \approx \rho_{12}^{SPA}(t) e^{-t/T_2^{SWAP}} \quad (57)$$

$$\rho_{03}(t) \approx \rho_{03}^{SPA}(t) e^{-\tilde{\Gamma}_{30}t}. \quad (58)$$

This result is confirmed by numerical solution of the stochastic Schrödinger equation for classical fluctuations leading to dynamical $1/f$ noise ($\gamma_m = 2\pi \times 1$ Hz and $\gamma_M = 2\pi \times (10^6 - 10^8)$ Hz). The evolution of populations is only due to quantum noise (in the adiabatic approximation they do not evolve), thus they are given by Eqs. (25) - (27) and the switching probabilities are given by Eqs. (38), (39) where $\rho_{ij}(t)$ are replaced by (57) and (58). These matrix elements enter also the concurrence which reads, for times $t \ll T_R$, $C(t) \approx \sqrt{(\rho_{11}(t) - \rho_{22}(t))^2 + (\text{Im}[2\rho_{12}(t)])^2} - |\sin \varphi| \rho_{00}(t)$.

The relevant time scales characterizing the efficiency of the \sqrt{i} -SWAP operation depend both on the SWAP coherence and on the populations of the first three levels. Due to the interplay of adiabatic and quantum noise, the time dependence is not a

\parallel This is analogous to a single qubit in the presence of adiabatic transverse noise, which is equivalent to longitudinal quadratic noise [44].

\blacklozenge In the multistage approach, the classical variables x_α and z_α enter parametrically also in the frequency shifts resulting from the solution of the Master Equation. Here we neglect this dependence, see Appendix C.

Table 5. Relaxation and decoherence times of the \sqrt{i} -SWAP gate and responsible physical processes (long-to-intermediate time behavior of $C(t)$ and of the switching probabilities).

Time scale	Physical origin
Relaxation to the ground state $T_R \approx 1/\Gamma_+$	Transverse noise at frequency Ω
SWAP relaxation time $T_1^{SWAP} \approx 1/\Gamma_-$	Longitudinal noise at frequency ω_{21}
SWAP decoherence time $T_2^{SWAP} \approx 2T_1^{SWAP}$	Longitudinal noise at frequency ω_{21}
SWAP dephasing time T_2^{SWAP*} $\rho_{21}^{SPA}(T_2^{SWAP*}) = e^{-1}$	Low frequency noise (longitudinal AND transverse)
SWAP total decoherence time $T_2^{SWAP} = [1/2T_1^{SWAP} + 1/T_2^{SWAP*}]^{-1}$	if $T_R \gg T_1^{SWAP}$ i. e. $S_x(\Omega) \ll S_z(\omega_{21})$

superposition of exponentials. We can distinguish two time regions: a asymptotic long-time regime and a intermediate-to-short time regime.

The asymptotic behavior is entirely due to populations relaxation to the ground state, it is exponential and takes place with the "global" relaxation time $T_R \approx 1/\Gamma_+$, resulting from "effective transverse" inter-doublet processes, whose order of magnitude is the spectrum of transverse fluctuations at frequencies of order Ω . In order to avoid leakage from the SWAP-subspace, any two-qubit operation has to take place on a time much shorter than T_R . This constraint also applies to the SWAP decoherence times. The intermediate-to-short time behavior, $t \ll T_R$, gives more relevant information on the gate performance. In this time regime, relevant quantities are populations and coherences in the SWAP subspace. We distinguish a intermediate time regime, characterized by $T_1^{SWAP} \approx 1/\Gamma_-$ and $T_2^{SWAP} = 2T_1^{SWAP} \approx 1/\tilde{\Gamma}_{12}$ due to *effective transverse* quantum noise inside this subspace, physically originated from longitudinal noise on each qubit. Adiabatic noise leads to additional decay of the SWAP coherence, $\rho_{12}(t) \approx \rho_{12}^{SPA}(t) e^{-t/T_2^{SWAP}}$. The resulting defocusing is analogous to a "pure dephasing" process, we may name the typical time scale T_2^{SWAP*} , defined as the time at which $|\rho_{21}^{SPA}(T_2^{SWAP*})| = e^{-1}$. The time T_2^{SWAP*} is found by numerical inversion of (49). The *intermediate-time* behavior of the two-qubit gate is characterized by $1/T_1^{SWAP}$ and $1/T_2^{SWAP} = 1/(2T_1^{SWAP}) + 1/T_2^{SWAP*}$, analogously to a two-state system. These time scales and the responsible processes are summarized in table 5.

On the other side, in a quantum information perspective, it is important to estimate the time behavior (of concurrence or of switching probabilities) at times of the order of $t_e = \pi/2\omega_c$, the first moment in which the entangled state is reached by free evolution. In order to generate entanglement within the SWAP subspace it is necessary that $t_e \ll T_2^{SWAP}$. It is therefore relevant to estimate the system behavior at short-times $t \ll T_2^{SWAP}$. Both for the concurrence and the switching probability, the SWAP-

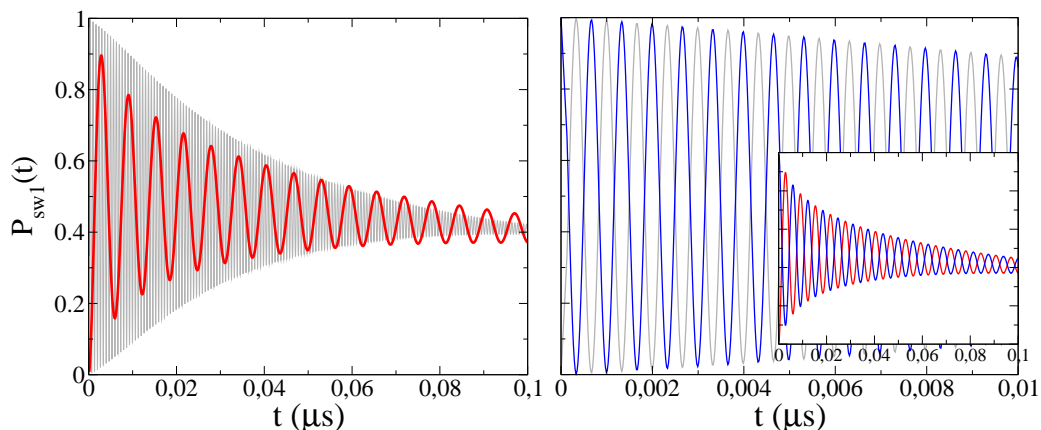


Figure 7. Qubit 1 switching probability $P_{\text{SW1}}(t)$ (red) and probability $P_2(t)$ (blue) to find qubit 2 in the initial state $|-\rangle$ in the presence of $1/f$ and white noise for $\omega_c/\Omega = 0.01$ and for optimal coupling $\tilde{\omega}_c = 0.08\Omega$ (gray). To emphasize the robustness of the optimal coupling choice here we consider $1/f$ charge noise of large amplitude, $\sigma_x = 8 \times 10^{-2}\Omega$. The remaining noise figures are those reported in table 3. Left panel: Plot of $P_{\text{SW1}}(t)$ showing the exponential short-time behavior at $\tilde{\omega}_c$ and the algebraic decay for generic coupling. Right panel: $P_{\text{SW1}}(t)$ and P_2 anti-phase oscillations for $\tilde{\omega}_c$ (main), $\omega_c/\Omega = 0.01$ (inset).

coherence rules the short-time limit which is approximately

$$|\rho_{12}| \propto 1 - \frac{t}{2T_1^{\text{SWAP}}} - \frac{1}{2} \Sigma_{21}^2 t^2. \quad (59)$$

The leading contribution, linear or quadratic, does not only depend on the noise amplitude but also on the operating point. In fact ω_c enters the SWAP-splitting variance Σ_{21} and, in principle, also the SWAP decoherence time due to quantum noise $2T_1^{\text{SWAP}}$. This is expected to be a smooth dependence. For the present considerations we assume a white spectrum in the relevant frequency range. For optimal coupling the short-time behavior is linear (since the effect of low frequency noise is considerably reduced) whereas for a different coupling strength the behavior is typically algebraic (see figure 7).

The short-time expansion is valid at t_e if $t_e \ll T_2^{\text{SWAP}}$. In figure 8 we consider two illustrative cases. For the expected noise characteristics as reported in table 3, for couplings $\Omega/100 < \omega_c < \Omega/10$ we have $\Sigma_{21}t_e < t_e/2T_1^{\text{SWAP}} \ll 1$. Thus the short-time expansion is valid up to t_e . Note that for the optimal coupling $1/2T_1^{\text{SWAP}}$ is about one order of magnitude larger than Σ_{21} (figure 8 left panel), thus $|\rho_{12}| \propto 1 - t/2T_1^{\text{SWAP}}$. For a larger amplitude of $1/f$ transverse noise, $\sigma_x \approx 0.08\Omega$, we have $t_e/2T_1^{\text{SWAP}} \leq \Sigma_{21}t_e \ll 1$ (figure 8 right panel). Also in this case the short-time expansion holds up to t_e . In this case however even for optimal coupling the linear and quadratic terms are comparable. The various possible short-times behaviors and validity regimes are summarized in table 6.

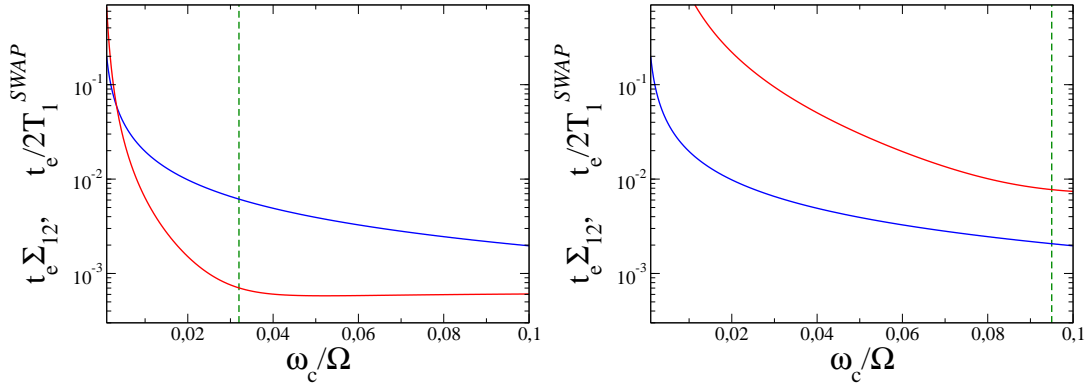


Figure 8. Plot of $\Sigma_{12}(\omega_c)t_e$ (red) and of $t_e/(2T_1^{SWAP})$ (blue) as a function of ω_c/Ω (logarithmic scale) for $\sigma_x/\Omega = 0.02$ (left panel) and $\sigma_x/\Omega = 0.08$ (right panel). The dashed line marks the optimal coupling Eq. (54).

Table 6. Short times behavior $t \ll T_2^{SWAP}$ of $C(t)$ and of the switching probabilities and validity conditions of the expansion up to t_e .

Short times expansion	Validity conditions	Expansion up to t_e if
$ \rho_{21}(t) \approx 1 - \frac{t}{2T_1^{SWAP}}$	Optimal coupling and $\Sigma_{21} \cdot 2T_1^{SWAP} < 1$	$\frac{t_e}{2T_1^{SWAP}} \ll 1$
$ \rho_{21}(t) \approx 1 - \frac{(\Sigma_{21}t)^2}{2}$	Generic coupling or $\Sigma_{21} \cdot 2T_1^{SWAP} > 1$	$\frac{t_e}{1/\Sigma_{21}} \ll 1$

7. Conclusions

In the present article we have identified the relevant decoherence times of an entangling operation due to the different decoherence channels originated from broad-band and non-monotonic noise affecting independently two qubits. Results depend on the interplay of noise at low and at high frequencies (with respect to both the single qubit splittings, Ω , and the qubits coupling strength, ω_c) and on the symmetries of the qubit-environment coupling Hamiltonian. In addition, "optimal" operating conditions for the universal two-qubit gate have been identified. Even if the relevant dynamics is within the SWAP subspace, the important time scales (both due to quantum and to adiabatic noise) can only be predicted considering the whole multilevel nature of the coupled systems.

In particular, relaxation processes from the SWAP subspace to the ground state only depend on *transverse* noise at frequency Ω . Decoherence processes internal to the SWAP subspace are instead originated from *longitudinal* noise at frequency ω_c . This apparently counter-intuitive result simply follows from the symmetries of the Hamiltonian expressed in the eigenbasis of coupled qubits, cfr eqs. (5) - (7). As a consequence, the conditions to generate entangled states within the SWAP-subspace involve the spectra of transverse and longitudinal fluctuations at two different frequencies. An efficient \sqrt{i} -SWAP operation can be realized when $S_{x\alpha}(\Omega) \ll S_{z\alpha}(\omega_c)$. The long-to-intermediate time behavior and the relevant decoherence times are summarized in table 5.

Defocusing processes instead originate both from transverse and longitudinal adiabatic noise. Remarkably, consideration of the coupled systems band structure allows identification of operating conditions of reduced sensitivity to low frequency fluctuations. An "optimal coupling" can be identified where defocusing is minimized. The error at the first $\sqrt{i - \text{SWAP}}$ operation at optimal coupling can be reduced of a factor of 4-to-10 with respect to operating at generic coupling strength. The possibility of optimal tuning is ultimately due to the absence of effective longitudinal noise in the SWAP-subspace and to the interplay of effective transverse intra- and inter-doublet fluctuations. The orthogonal Z-subspace instead, because of the presence of effective longitudinal noise, turns out to be much more sensitive to low-frequency noise which cannot be limited by properly choosing system parameters. Therefore, populating this subspace may severely limit the gate efficiency.

The short-times behavior of the relevant dynamical quantities crucially depends on adiabatic noise and its interplay with quantum noise. The dependence turns from quadratic to linear depending on the largest component, parametrized by the SWAP-splitting variance resulting from adiabatic noise, Σ_{21} , and the SWAP-decoherence rate due to quantum noise $[2T_1^{\text{SWAP}}]^{-1}$, as summarized in table 6.

The considerable protection from 1/f noise achievable in the SWAP-subspace for optimal coupling may suggest to use this subspace to encode a single quantum bit, similarly to a decoherence-free-subspace [45]. Such an encoding would be convenient if the SWAP decoherence time was about two orders of magnitude larger than the qubit decoherence time T_2 . In fact, because of the smaller SWAP oscillation frequency, $\omega_c \approx 10^{-1(-2)}\Omega$, the quality factor of a single qubit rotation within this subspace would be $Q = T_2^{\text{SWAP}}\omega_c \approx 10^{-1(-2)}T_2^{\text{SWAP}}\Omega$, therefore $Q \gg T_2\Omega$ if $T_2^{\text{SWAP}} \gg 10^{1(2)}T_2$. Realizing this condition requires improving the relaxation times with respect to present day experiments. A more realistic possibility is instead to employ the SWAP subspace as a single qubit quantum memory. The requirement in this case would be satisfying the weaker condition, $T_2^{\text{SWAP}} > T_2$.

Finally, we would like to comment on the effects of selected impurities strongly coupled to the two-qubit gate. The detrimental effect of charged bistable fluctuators on single qubit charge or charge-phase gates has been observed in experiments [2, 3] and explained in theory [22, 36]. Effects on a two-qubit gate may even be worse, as reported in the recent experiment on two coupled quantronium [38]. Explanation of the rich physics which comes out when selected impurities couple to the nano-device is beyond the scope of the present article. In the following Appendix B, we illustrate the possible scenario when an impurity considerably changes the 4-level spectrum of the coupled qubits and we speculate on the possibility to limit its effects by proper tuning the system parameters, somehow extending the optimal tuning recipe. The usefulness of such a choice however critically depends on the interplay with quantum noise at intermediate frequencies, an information unavailable in present day experiments. The analysis in Appendix B is the first step towards the identification of parameter regimes where a multilevel nano-device may be protected also from strongly coupled degrees of

freedom of a structured bath.

Acknowledgments

Stimulating discussions with G. Schön and U. Weiss are gratefully acknowledged.

Appendix A. Capacitively coupled Cooper-Pair-Box based qubits

The Hamiltonian \mathcal{H}_0 in Eq. (1) is the central model of any non trivial two-qubit gate based on a fixed coupling scheme. In particular, it describes coupled superconducting qubits in the various implementations [5]. With \mathcal{H}_1 , given in (2), it includes independent fluctuations responsible for incoherent processes of different physical origin. In this Section we derive $\mathcal{H}_0 + \mathcal{H}_1$ for capacitive coupled Cooper-Pair-Box-based (CPB) nano-devices. The CPB is the main building block of many superconducting qubits [46]. Here we consider two charge-phase qubits (quantronia) [3] electrostatically coupled via a fixed capacitor, as schematically illustrated in figure A1.

Each qubit is operated via two control parameters, the gate voltage V_g and the magnetic flux across the junction loop, Φ_x . They enter the CPB Hamiltonian via the dimensionless parameters $q_x = C_g V_g / (2e)$ and $\delta = \pi \Phi_x / \Phi_0$:

$$\mathcal{H}_{\text{CPB}} = E_C^0 (\hat{q} - q_x)^2 - E_J(\delta) \cos \hat{\varphi}, \quad (\text{A.1})$$

here $E_C^0 = 2e^2 / C_\Sigma$ and $E_J(\delta) = E_J^0 \cos \delta$ is the Josephson energy, modulated by the phase δ around the zero phase value E_J^0 . Charge \hat{q} and phase $\hat{\varphi}$ are conjugate operators, $[\hat{\varphi}, \hat{q}] = i$. The loop capacitance C_Σ is the sum of the gate C_g and the junctions C_J capacitances. The two CPBs are coupled by inserting a fixed capacitance C_C between the two islands. The presence of the coupling capacitance leads to a renormalization of the CPB charging energies $E_{\alpha,C} = E_{\alpha,C}^0 (1 - C_T / C_{\alpha,\Sigma})$, being $E_{\alpha,C}^0$ the CPB charging energy of the uncoupled qubit α , $1/C_T = 1/C_C + 1/C_{1,\Sigma} + 1/C_{2,\Sigma}$ the total inverse capacitance of the device. The coupling energy is $E_{CC} = (2e)^2 C_T / (C_{1,\Sigma} C_{2,\Sigma})$, and the full device Hamiltonian reads

$$\mathcal{H}_D = \mathcal{H}_{\text{CPB1}} \otimes \mathbb{I}_2 + \mathbb{I}_1 \otimes \mathcal{H}_{\text{CPB2}} + \mathcal{H}_C \quad (\text{A.2})$$

$$\mathcal{H}_{\text{CPB}\alpha} = E_{\alpha,C} [\hat{q}_\alpha - q_{\alpha,x} \mathbb{I}_\alpha]^2 - E_{\alpha,J}(\delta_\alpha) \cos \hat{\varphi}_\alpha,$$

$$\mathcal{H}_C = E_{CC} [\hat{q}_1 - q_{1,x} \mathbb{I}_1] \otimes [\hat{q}_2 - q_{2,x} \mathbb{I}_2], \quad (\text{A.3})$$

where the control parameters $q_{\alpha,x}$ and δ_α , and the charge \hat{q}_α and phase operators $\hat{\varphi}_\alpha$ play the same role as in the single qubit case. At sufficiently low temperatures, the evolution of each CPB approximately takes place within the bi-dimensional subspace spanned by the lowest energy eigenstates of $\mathcal{H}_{\text{CPB}\alpha}$, $|\pm\rangle_\alpha$ with a splitting depending on the control parameters [47], $\mathcal{H}_\alpha = \mathcal{P}_\alpha \mathcal{H}_{\text{CPB}\alpha} \mathcal{P}_\alpha = -\frac{1}{2} \Omega_\alpha \sigma_{\alpha z}$, where the projection operator reads $\mathcal{P}_\alpha = |\alpha\rangle\langle\alpha| + |-\alpha\rangle\langle-\alpha|$ and $\sigma_{\alpha z} = |\alpha\rangle\langle\alpha| - |-\alpha\rangle\langle-\alpha|$. The restricted dynamics of the coupled CPBs can be described in a pseudo-spin formalism by projection in the eigenstates basis $\{|\mu, \nu\rangle = |\mu_1\rangle \otimes |\nu_2\rangle\}$. In this subspace the charge and

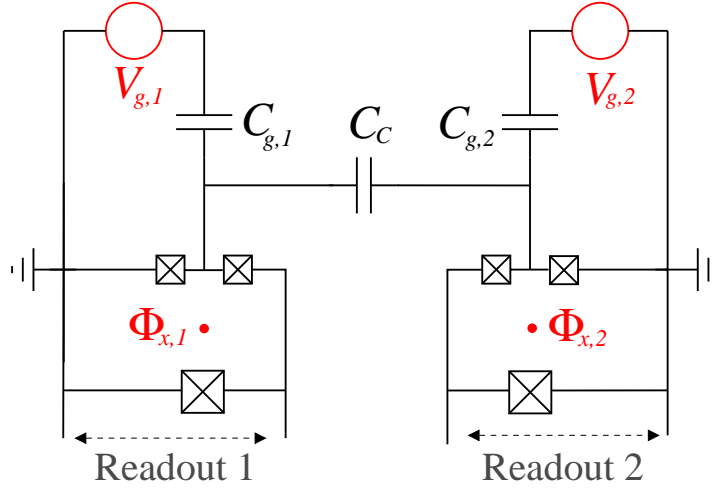


Figure A1. Electrical circuit of two quantronia, labeled as 1 and 2, coupled via a fixed capacitor C_C . Each qubit has the characteristic two-port design, with control parameters the gate voltage $V_{g,\alpha}$ and the magnetic flux $\Phi_{x,\alpha}$ threading the superconducting loop [3].

Josephson operators are expressed in terms both of $\sigma_{\alpha z}$ and of the transverse component $\sigma_{\alpha x} = |\alpha\rangle\langle -|\alpha + \alpha\rangle\langle +|\alpha$ as follows

$$\mathcal{P}_\alpha \hat{q}_\alpha \mathcal{P}_\alpha = -\frac{1}{2}(q_{\alpha,++} - q_{\alpha,--})\sigma_{\alpha z} + q_{\alpha,+} \sigma_{\alpha x} + \frac{1}{2}(q_{\alpha,++} + q_{\alpha,--})\mathbb{I}_\alpha \quad (\text{A.4})$$

$$\mathcal{P}_\alpha (\cos \hat{\varphi}_\alpha) \mathcal{P}_\alpha = -\frac{1}{2}(\Phi_{\alpha,++} - \Phi_{\alpha,--})\sigma_{\alpha z} + \Phi_{\alpha,+} \sigma_{\alpha x} + \frac{1}{2}(\Phi_{\alpha,++} + \Phi_{\alpha,--})\mathbb{I}_\alpha, \quad (\text{A.5})$$

where

$$q_{\alpha,\mu\nu} = q_{\alpha,\nu\mu} = {}_\alpha\langle \mu | \hat{q}_\alpha | \nu \rangle_\alpha \quad \Phi_{\alpha,\mu\nu} = \Phi_{\alpha,\nu\mu} = {}_\alpha\langle \mu | \cos \hat{\varphi}_\alpha | \nu \rangle_\alpha.$$

The restriction of the device Hamiltonian to $\{|\mu, \nu\rangle\}$ is ⁺

$$\begin{aligned} (\mathcal{P}_1 \otimes \mathcal{P}_2) \mathcal{H}_D (\mathcal{P}_1 \otimes \mathcal{P}_2) &\equiv \tilde{\mathcal{H}}_D = - \sum_\alpha \frac{\Omega_\alpha}{2} \sigma_{\alpha z} + \\ &+ \frac{E_{CC}}{2} \sum_{\alpha \neq \beta} \left[-\frac{1}{2}(q_{\alpha,++} - q_{\alpha,--})\sigma_{\alpha z} + q_{\alpha,+} \sigma_{\alpha x} \right] (q_{\beta,++} + q_{\beta,--} - 2q_{\beta,x}) \\ &+ E_{CC} \prod_\alpha \left[-\frac{1}{2}(q_{\alpha,++} - q_{\alpha,--})\sigma_{\alpha z} + q_{\alpha,+} \sigma_{\alpha x} \right] \end{aligned} \quad (\text{A.6})$$

Note that because of the coupling, in addition to interaction terms between the two qubits, each qubit is effectively displaced from its own operating point (second term in (A.6)).

Because of fluctuations of control parameters the device couples to the external environment. The form of interaction terms can be easily deduced considering classical fluctuations of $q_{\alpha,x}$ and δ_α , i.e. by replacing in (A.2) and (A.3), $q_{\alpha,x} \rightarrow q_{\alpha,x} + \Delta q_{\alpha,x}$ and $\delta_\alpha \rightarrow \delta_\alpha + \Delta \delta_\alpha$. We therefore obtain $\mathcal{H}_D \rightarrow \mathcal{H}_D + \delta \mathcal{H}_D$, where

$$\delta \mathcal{H}_D = \delta \mathcal{H}_{\text{CPB1}} \otimes \mathbb{I}_2 + \mathbb{I}_1 \otimes \delta \mathcal{H}_{\text{CPB2}} + \delta \mathcal{H}_C.$$

⁺ We have used the shorthand notation σ_α to indicate $\sigma_\alpha \otimes \mathbb{I}_\beta$, $\alpha \neq \beta$.

Fluctuations of each CPB Hamiltonian and of the coupling term read

$$\delta\mathcal{H}_{\text{CPB}\alpha} = X_\alpha \hat{q}_\alpha + Z_\alpha \cos \hat{\varphi}_\alpha \quad (\text{A.7})$$

$$\delta\mathcal{H}_C = g_2 X_2 \hat{q}_1 \otimes \mathbb{I}_2 + g_1 X_1 \mathbb{I}_1 \otimes \hat{q}_2, \quad (\text{A.8})$$

where X_α is related to gate charge fluctuations, $X_\alpha = -2E_{\alpha,C}\Delta q_{\alpha,x}$ and Z_α to fluctuations of the phase or equivalently of the Josephson energy, $Z_\alpha = -\Delta E_{\alpha,J}$, where $\Delta E_{\alpha,J} = E_{\alpha,J}(\delta_\alpha + \Delta\delta_\alpha) - E_{\alpha,J}(\delta_\alpha)$, and we put $g_\alpha = E_{CC}/(2E_{\alpha,C})$. In the computational subspace the additional terms reduce to

$$\begin{aligned} \delta\mathcal{H}_\alpha = & -\frac{1}{2}X_\alpha(q_{\alpha,++} - q_{\alpha,--})\sigma_{\alpha z} + X_\alpha q_{\alpha,+} \sigma_{\alpha x} + \frac{1}{2}X_\alpha(q_{\alpha,++} + q_{\alpha,--})\mathbb{I}_\alpha \\ & -\frac{1}{2}Z_\alpha(\Phi_{\alpha,++} - \Phi_{\alpha,--})\sigma_{\alpha z} + Z_\alpha\Phi_{\alpha,+} \sigma_{\alpha x} + \frac{1}{2}Z_\alpha(\Phi_{\alpha,++} + \Phi_{\alpha,--})\mathbb{I}_\alpha \end{aligned} \quad (\text{A.9})$$

and

$$\begin{aligned} \delta\mathcal{H}_C = & g_2 X_2 \left[-\frac{1}{2}(q_{1,++} - q_{1,--})\sigma_{1z} + q_{1,+} \sigma_{1x} + \frac{1}{2}(q_{1,++} + q_{1,--})\mathbb{I}_1 \right] \otimes \mathbb{I}_2 \\ & + g_1 X_1 \mathbb{I}_1 \otimes \left[-\frac{1}{2}(q_{2,++} - q_{2,--})\sigma_{2z} + q_{2,+} \sigma_{2x} + \frac{1}{2}(q_{2,++} + q_{2,--})\mathbb{I}_2 \right]. \end{aligned} \quad (\text{A.10})$$

In conclusion, the coupled CPBs Hamiltonian at a general working point, in the four dimensional subspace $\{|\mu, \nu\rangle\}$, including fluctuations of the control parameters and neglecting constant terms, takes the form $\tilde{\mathcal{H}}_D + \delta\tilde{\mathcal{H}}_D$ with $\tilde{\mathcal{H}}_D$ given in eq. (A.6) and

$$\begin{aligned} \delta\tilde{\mathcal{H}}_D = & \sum_\alpha \left[\frac{1}{2}(X_\alpha(q_{\alpha,--} - q_{\alpha,++}) + Z_\alpha(\Phi_{\alpha,--} - \Phi_{\alpha,++}))\sigma_{\alpha z} + (X_\alpha q_{\alpha,+} + Z_\alpha\Phi_{\alpha,+})\sigma_{\alpha x} \right] \\ & + g_2 X_2 \left[\frac{1}{2}(q_{1,--} - q_{1,++})\sigma_{1z} + q_{1,+} \sigma_{1x} \right] + g_1 X_1 \left[\frac{1}{2}(q_{2,--} - q_{2,++})\sigma_{2z} + q_{2,+} \sigma_{2x} \right] \end{aligned} \quad (\text{A.11})$$

Note that due to the capacitive coupling a cross-talk effect takes place, gate charge fluctuations of qubit α being responsible for fluctuations of the polarization of qubit β . Effects are scaled with the coupling energy E_{CC} , thus they are expected to be less relevant compared to fluctuations acting directly on each qubit. A detailed analysis of cross-talk and correlations between gate charge fluctuations has been reported in [33]. In our analysis we disregarded cross-talk and correlations between noise sources acting on each qubit.

Appendix A.1. Choice of the working point

The implementation of a two qubit gate in a fixed coupling scheme requires the qubits to be at resonance during gate operation. Because of experimental tolerances on bare parameters (about 10%), the resonant condition can only be achieved by a proper choice of the single-qubit working points via tuning $q_{\alpha,x}$ and δ_α . This is a critical choice since at least one qubit has to be moved away from the working point of minimal sensitivity to parameters variations, the "optimal point", $q_{\alpha,x} = 1/2$, $\delta_\alpha = 0$ [3]. Since CPB-based devices are severely affected by low-frequency charge noise it is desirable to maintain the charge optimal point, $q_{\alpha,x} = 1/2$ and modulate resonance/detuning by tuning the

Table A1. Typical values of the CPBs parameters [38]. Ω^0 is the energy splitting of the single qubit.

Parameter	Qubit 1	Qubit 2
E_C^0 (GHz)	9.997	10.41
E_J^0 (GHz)	14.16	15.62
C_Σ (fF)	7.73	7.42
Ω^0 (GHz)	12.666	13.81
$E_{\alpha,C}$ (GHz)	9.92	10.33
Ω (GHz)	12.645	13.79

Table A2. Matrix elements of the charge and Josephson operators in the two lowest eigenstates basis of each CPB Hamiltonian. The physical parameters of each CPB are given in table A1.

	Qubit 1	Qubit 2
$\tilde{q}_{\alpha,++} - \tilde{q}_{\alpha,--}$	0	0
$\tilde{q}_{\alpha,+}$	-0.5962161	-0.5891346
$\tilde{\Phi}_{\alpha,++} - \tilde{\Phi}_{\alpha,--}$	0.7049074	0.7396952
$\tilde{\Phi}_{\alpha,+}$	0	0

phases δ_α . The most reasonable choice consists in maintaining one qubit at its own phase optimal point, $\delta_1 = 0$ and tune the phase of the other qubit, δ_2 . For set of parameters close to those planned in experiments [38] (see table A1) resonance occurs for $\delta_2 \approx 0.455$. Since at $q_{\alpha,x} = 1/2$ it results $q_{\alpha,++} = q_{\alpha,--} = 1/2$ and $\Phi_{\alpha,+} = 0$, the projected charge (A.4) is transverse and the Josephson operator (A.5) is longitudinal with respect to each Hamiltonian \mathcal{H}_α . Therefore, the truncated Hamiltonian is of the form $\mathcal{H}_0 + \mathcal{H}_I$ given by eqs. (1) and (2) respectively

$$\mathcal{H}_0 = -\frac{\Omega}{2} \sigma_{1z} \otimes \mathbb{I}_2 - \frac{\Omega}{2} \mathbb{I}_1 \otimes \sigma_{2z} + E_{CC} \tilde{q}_{1,+} - \tilde{q}_{2,+} \sigma_{1x} \otimes \sigma_{2x} \quad (\text{A.12})$$

$$\delta\mathcal{H}_0 = \sum_{\alpha \neq \beta} \left[\frac{1}{2} Z_\alpha (\tilde{\Phi}_{\alpha,--} - \tilde{\Phi}_{\alpha,++}) \sigma_{\alpha z} + X_\alpha \tilde{q}_{\alpha,+} \sigma_{\alpha x} \right] \otimes \mathbb{I}_\beta \quad (\text{A.13})$$

where $\tilde{q}_{\alpha,+}$, $\tilde{\Phi}_{\alpha,++}$ etc. denote the specific values taken by these matrix elements at the resonance point obtained for a specific choice of δ_2 . Values of the charge and phase matrix elements at this working point are reported in table A2 and lead to $E_{CC} = 0.18$ GHz. The interaction Hamiltonian \mathcal{H}_I results from $\delta\mathcal{H}_0$ considering the quantized version of the classical fluctuations $x_\alpha = -4E_{\alpha,C} \tilde{q}_{\alpha,+} - \Delta q_{\alpha,x}$ and $z_\alpha = (\tilde{\Phi}_{\alpha,++} - \tilde{\Phi}_{\alpha,--}) \Delta E_{\alpha,J}$. Where, since $\delta_1 = 0$ we have $\Delta E_{1,J} = -0.5 E_{1,J}^0 (\Delta \delta_1)^2$ whereas for $\delta_2 \neq 0$ it results $\Delta E_{2,J} = -E_{2,J}^0 (\sin \delta_2) \Delta \delta_2$.

The accuracy of the truncation of the multistate device Hamiltonian to the lowest four eigenstates has been checked numerically by exact diagonalization of (A.2) using the numerical values of the physical parameters reported in table A1 and considering 14 charge states for each qubit, see figure A2.

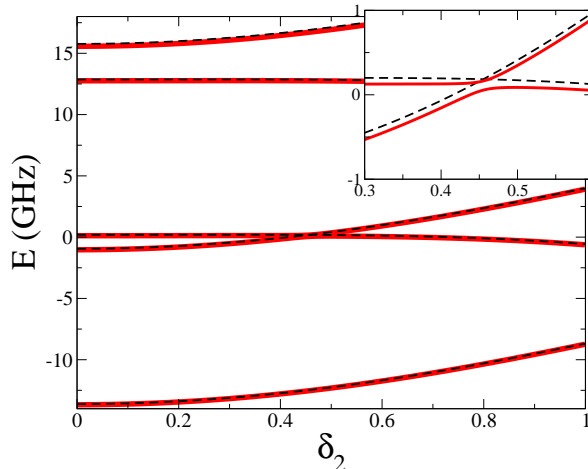


Figure A2. The five lowest eigenenergies of the coupled two CPB Hamiltonian (A.2) at charge optimal points $q_{1,x} = q_{2,x} = 1/2$ versus the qubit 2 phase δ_2 , being $\delta_1 = 0$. The dashed black and red lines refer to the uncoupled and coupled case, respectively. The 5-th eigenvalue lies sufficiently far in energy to be neglected in our analysis. In the inset the degeneracy point is shown with the small anti-crossing due to the coupling term at $\delta_2 = 0.455$.

Appendix A.2. Structured noise in CPB-based circuits

Fluctuations of the control parameters $q_{\alpha,x}$, δ_α have different physical origin. They partly stem from microscopic noise sources, partly from the circuitry itself. The resulting stochastic processes are sometimes non-Gaussian, therefore complete characterization of the processes requires in principle higher-order cumulants. Such a complete description is often unavailable in experiments, whereas it is usually possible to provide a characterization of the power spectrum of the various stochastic processes. Noise characteristics for the two quantronia are summarized in table 3 (section 4).

Experiments on various Josephson implementations have revealed the presence of spurious resonances in the spectrum which manifest themselves as beatings in time resolved measurements [3]. In charge and charge-phase qubits they are due to strongly coupled (SC) background charges and may severely limit the reliability of these devices [35, 36]. In the following Appendix B we will discuss the detrimental effect of a single strongly-coupled impurity on the visibility of a $\sqrt{i - \text{SWAP}}$ operation.

Finally, we mention that in the present analysis we have not explicitly considered fluctuations of the Josephson energy due to critical current fluctuations. The effect of E_J^0 noise may be straightforwardly included in our analysis within the multistage approach.

Appendix B. Effect of a strongly coupled impurity

Experiments on various Josephson implementations have revealed the presence of spurious resonances in the spectrum which manifest themselves as beatings in time resolved measurements [3, 15, 16, 21]. In charge and charge-phase qubits they are due

to strongly coupled (SC) background charges and may severely limit the reliability of these devices [35, 36]. Several experiments have shown that these impurities can be modeled as bistable fluctuators (BF), switching between states 0 and 1 with a rate γ . Often the qubit-BF coupling is transverse, i.e. of the form $-(v/2)\sigma_x\xi(t)$ with $\xi(t) = \{0, 1\}$ [48]. Each bistable state corresponds to a different qubit splitting, Ω for $\xi = 0$ and $\Omega' \approx \Omega[1 + 0.5(v/\Omega)^2]$ for $\xi = 1$ ($v \ll \Omega$). The parameter quantifying the strength of the qubit-BF coupling is $g_1 \equiv (\Omega' - \Omega)/\gamma$ [35]. When $g_1 \gg 1$ the impurity is strongly coupled and it is visible both in spectroscopy and in the time-resolved dynamics. Similarly, a single BF acting on one of the two qubits forming a universal gate induces a bi-stability in the SWAP-splitting: $\omega_{21} = \omega_c$ for $\xi = 0$ and $\omega'_{21} \approx \omega_c[1 - 0.5(v/\Omega)^2 + v^4/(8\omega_c^2\Omega^2)]$ for $\xi = 1$ (in this case the stronger condition on the qubit-BF coupling has been assumed $v \ll \omega_c$). The strong coupling condition for the \sqrt{i} -SWAP gate is therefore $g_2 = (\omega'_{21} - \omega_{21})/\gamma \gg 1$. Considering the above expansions and the constraint $\Omega > \omega_c$ the two ratios satisfy the condition $g_1 > g_2$. Therefore the visibility of a specific BF is expected to be reduced in a two-qubit operation with respect to a single qubit gate.

The effect of a single BF fluctuator depends on the way experimental data are collected. For spectroscopic measurements the single-shot time is about 200 ns and the acquisition time of a single point in the spectrum requires about 4×10^4 repetitions, resulting in a recording time for a single data point of about 10^{-2} s [38]. Therefore a single BF will be visible in spectroscopy if its switching time is 0.5×10^{-7} s $< 1/\gamma < 2 \times 10^{-2}$ s. For instance a BF switching at ≈ 10 kHz can be averaged during the spectroscopic measurements and it is visible if it is sufficiently strongly coupled to one qubit, for instance this is the case for $v/\Omega = 0.1 > \omega_c/\Omega$. The expected effect of this impurity in spectroscopy is shown in figure B1 where it results in the simultaneous presence of two avoided crossings depending on the impurity state. The occurrence of a similar BF represents a major problem for charge and charge-phase implementations [38]. Effects are also visible in time resolved measurements. If the considered BF is one out of the several ones responsible for $1/f$ noise, the global effect of the structured bath is a considerable reduction of the oscillation amplitude, as shown in figure B1. Under these conditions, in principle, an "optimal coupling" can still be identified. Since the main problem is the beating pattern, optimal tuning is defined by the condition that the average $\langle \omega'_{21} - \omega_{21} \rangle$ vanishes, rather than minimizing the SWAP-splitting variance. In the presence of only charge noise, this condition leads to a modified "optimal coupling", $\tilde{\omega}_c = \sqrt{\sigma_x^2 + v^2/4}$, at which effectively the SWAP visibility is improved (figure B1). The efficiency of such a choice however critically depends on the details (presently not available) of transverse noise at frequencies in the kHz - MHz range. Relaxation processes due to quantum noise at these frequencies may in fact represent an additional limiting factor for the gate fidelity.

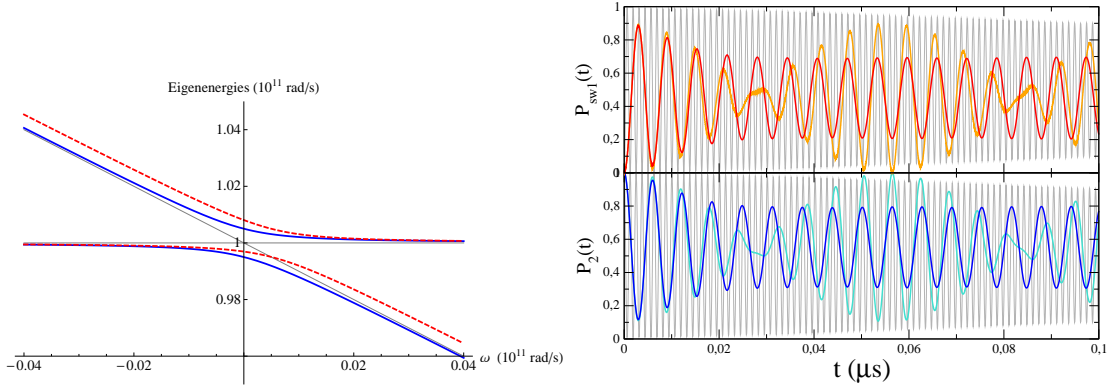


Figure B1. Left: Simulated spectroscopy of the SWAP splitting ω_{21} for qubit-qubit coupling $\omega_c/\Omega = 0.01$ (blue) and for uncoupled qubits (black). In the presence of a BF coupled to one qubit with strength $v/\Omega = 0.1$ the coupled qubits ($\omega_c/\Omega = 0.01$) eigenenergies are shifted (red). Right: Numerical simulations of the switching probabilities in the presence of the above BF (orange/cyan), and of the BF plus $1/f$ noise with $\sigma_x = 0.02\Omega$ (blue and red). For optimal coupling, $\tilde{\omega}_c = \sqrt{\sigma_x^2 + v^2/4}$, a considerable recover of the signal can be obtained (gray).

Appendix C. Frequency shifts

In this Appendix we report the frequency shifts entering the off-diagonal elements of the RDM as resulting from the solution of the Master Equation in the secular approximation reported in section 4. The frequency shifts take the simple form

$$\begin{aligned} \tilde{\omega}_{12} - \omega_{12} &= \frac{1}{2} \left[\sum_{k \neq 2} \mathcal{E}_{2k} - \sum_{k \neq 1} \mathcal{E}_{1k} \right] \\ \tilde{\omega}_{03} - \omega_{03} &= \frac{1}{2} \left[\sum_{k \neq 0} \mathcal{E}_{0k} - \sum_{k \neq 3} \mathcal{E}_{3k} \right]. \end{aligned} \quad (\text{C.1})$$

For the SWAP coherence the different contributions read

$$\begin{aligned} \mathcal{E}_{10} &= \frac{1}{8} (1 + \sin \varphi) [\mathcal{E}_{x_1}(\omega_{10}) + \mathcal{E}_{x_2}(\omega_{10})] \\ \mathcal{E}_{13} &= \frac{1}{8} (1 - \sin \varphi) [\mathcal{E}_{x_1}(\omega_{13}) + \mathcal{E}_{x_2}(\omega_{13})] \\ \mathcal{E}_{20} &= \frac{1}{8} (1 - \sin \varphi) [\mathcal{E}_{x_1}(\omega_{20}) + \mathcal{E}_{x_2}(\omega_{20})] \\ \mathcal{E}_{23} &= \frac{1}{8} (1 + \sin \varphi) [\mathcal{E}_{x_1}(\omega_{23}) + \mathcal{E}_{x_2}(\omega_{23})] \\ \mathcal{E}_{21} &= \frac{1}{8} \{ [\mathcal{E}_{z_1}(\omega_{21}) + \mathcal{E}_{z_2}(\omega_{21})] \} \\ \mathcal{E}_{12} &= \frac{1}{8} \{ [\mathcal{E}_{z_1}(\omega_{12}) + \mathcal{E}_{z_2}(\omega_{12})] \} \end{aligned}$$

From single qubit measurements, as reported in section Appendix A.2, charge noise at frequencies of order of Ω is white. Assuming that also the phase variables $\Delta\delta_\alpha$ have white spectrum at frequencies of order ω_c , results in $S_{z_2}(\omega) = (E_{J,2}^0 \sin \delta_2)^2 S_{\delta_2}(\omega) \approx 5 \times 10^7 \text{s}^{-1}$. The spectrum of \hat{z}_1 takes instead the ohmic form $S_{z_1}(\omega) = 2S^2/(\pi\Omega^2)\omega \coth(\omega/(2K_B T))$, where $S = 1.6 \times 10^8 \text{s}^{-1}$. Under these

conditions, phase shifts due to polarization noise and phase fluctuations on qubit 2 identically vanish (from (19)). A frequency shift contribution results from ohmic phase noise on qubit 1, similarly to a qubit affected by transverse noise [23], as it can be argued from (5)

$$\tilde{\omega}_{12} - \omega_{12} = \frac{1}{8} [\mathcal{E}_{z_1}(\omega_{21}) - \mathcal{E}_{z_1}(-\omega_{21})] = \mathcal{P} \int_{-\infty}^{\infty} \frac{d\omega}{4\pi} \frac{S_{z_1}(\omega)}{1 + e^{-\omega/k_B T}} \frac{\omega_{21}}{\omega^2 - \omega_{21}^2}. \quad (\text{C.2})$$

The shift depends on the high-frequency cut-off of the spectrum and on the temperature. Explicit forms are known in the literature, see [23]. The damping strength parameter entering the ohmic spectrum, commonly denoted as K , is in the present case $K = S^2/(\pi\Omega^2) \approx 10^{-6}$. The SWAP-splitting shift scales with K and it will therefore be extremely small. Possible logarithmic divergences with the high-frequency cut-off are not included in this analysis since there's presently no indication on the features of the spectrum at those frequencies. For this reason frequency shifts have been neglected both in Section 4 and in Section 5.

References

- [1] M. Nielsen, I. Chuang, "Quantum Computation and Quantum Information", Cambridge Univ. Press, 2005.
- [2] Y. Nakamura *et al.*, Nature **398**, 786 (1999); Y. Yu *et al.*, Science **296**, 889 (2002); J. M. Martinis *et al.*, Phys. Rev. Lett. **89**, 117901 (2002); I. Chiorescu *et al.*, Science, **299**, 1869, (2003); T. Yamamoto *et al.*, Nature **425**, 941 (2003); S. Saito *et al.*, Phys. Rev. Lett. **93**, 037001 (2004); J. Johansson *et al.*, *ibid.* **96**, 127006 (2006); F. Deppe *et al.*, Nat. Phys. **4**, 686 (2008); J. A. Schreier *et al.*, Phys. Rev. B **77**, 180502(R) (2008).
- [3] D. Vion *et al.*, Science **296**, 886 (2002).
- [4] J. Clarke, F. K. Wilhelm, Nature **453**, 1031 (2008) and references therein.
- [5] Yu. A. Pashkin *et al.*, Nature **421**, 823 (2003); A. J. Berkley *et al.*, Science **300**, 1548 (2003); T. Yamamoto *et al.*, Nature **425**, 941 (2003); J. B. Majer *et al.*, Phys. Rev. Lett. **94**, 090501 (2005); J. H. Plantenberg *et al.*, Nature **447**, 836 (2007).
- [6] A. Izmailkov *et al.*, Phys. Rev. Lett. **93**, 037003 (2004); T. Hime *et al.*, Science **314**, 1427 (2006); A. O. Niskanen *et al.*, Science **316**, 723 (2007); M. A. Sillanpää *et al.*, Nature **449**, 438 (2007); J. Majer *et al.*, Nature **449**, 443 (2007); S. H. W. van der Ploeg *et al.*, Phys. Rev. Lett. **98**, 057004 (2007); A. Fay *et al.*, Phys. Rev. Lett. **100**, 187003 (2008).
- [7] M. Ansmann *et al.* Nature **461**, 504 (2009); A. Palacios-Laloy *et al.* Nature Physics **1641**, 504 (2009)
- [8] R. McDermott *et al.*, Science **307**, 1299 (2005); M. Steffen *et al.*, Science **313**, 1423 (2006).
- [9] L. DiCarlo *et al.* Nature **460**, 240 (2009).
- [10] M. Neeley *et al.*, Nature **467**, 570 (2010); L. DiCarlo *et al.*, Nature **467**, 574 (2010).
- [11] Y. Nakamura *et al.*, Phys. Rev. Lett. **88**, 047901 (2002).
- [12] O. Astafiev *et al.*, Phys. Rev. Lett. **93**, 267007 (2004).
- [13] G. Ithier *et al.*, Phys. Rev. B **72**, 134519 (2005).
- [14] J. Bylander *et al.* Nat. Phys. (2011), DOI:10.1038/NPHYS1994
- [15] R. W. Simmonds *et al.*, Phys. Rev. Lett. **93**, 077003 (2004).
- [16] P. Bushev *et al.*, Phys. Rev. B **82**, 134530 (2010).
- [17] S. Kafanov *et al.*, Phys. Rev. B **78**, 125411 (2008).
- [18] Roger H. Koch *et al.* Phys. Rev. Lett. **98**, 267003 (2007).
- [19] D. J. Van Harlingen *et al.* Phys. Rev. B **70**, 064517 (2004).
- [20] Radoslaw C. Bialczak *et al.*, Phys. Rev. Lett. **99**, 187006 (2007).

- [21] B. L. T. Plourde *et al.* Phys. Rev. B **72**, 060506(R) (2005); Z. Kim *et al.* Phys. Rev. B **78**, 144506 (2008); E. Hoskinson *et al.* Phys. Rev. Lett. **102**, 097004 (2009); A. Lupascu *et al.* Phys. Rev. B **80**, 172506 (2009); J. Lisenfeld *et al.*, Phys. Rev. B **81**, 100511(R) (2010).
- [22] G. Falci *et al.*, Phys. Rev. Lett. **94**, 167002 (2005).
- [23] U. Weiss, *Quantum Dissipative Systems*, Series in Modern Condensed Matter Physics-Vol. 13, (World Scientific, Singapore, 3rd enlarged edition, 2008).
- [24] C. P. Schlichter, *Principles of Magnetic Resonance* (Springer, New York, 1996).
- [25] M. Governale, M. Grifoni, G. Schön, Chem. Phys. **268**, 273 (2001); M. J. Storcz and F. K. Wilhelm, Phys. Rev. A **67**, 042319 (2003); M. J. Storcz *et al.*, Phys. Rev. A **72**, 052314 (2005); T. Ojanen *et al.* Phys. Rev. B **76**, 100505 (2007); G. Campagnano, A. Hamma and U. Weiss, Phys. Lett. A **374**, 416 (2010).
- [26] M. Thorwart, P. Hänggi, Phys. Rev. A **65**, 012309 (2002).
- [27] P. Nägele, G. Campagnano and U. Weiss, New J. Phys. **10**, 115010 (2008).
- [28] W. K. Wothers Phys. Rev. Lett. **80**, 2245 (1998).
- [29] D.V. Averin, C. Bruder, Phys. Rev. Lett. **91**, 057003 (2003); A. Blais *et al.*, Phys. Rev. Lett. **90**, 127901 (2003); F. Plastina, G. Falci, Phys. Rev. B **67**, 224514 (2003); B.Plourde *et al.*, Phys. Rev. B **70**, 140501(R) (2004); A.O. Niskanen, Y. Nakamura, J.S. Tsai, Phys. Rev. B **73**, 094506 (2006); P. Bertet, C. J. Harmans, J.E. Mooij, Phys. Rev. B **73**, 064512 (2006); Y-D Wang, A. Kemp, K. Semba, Phys. Rev. B **79**, 024502 (2009); R. A. Pinto *et al.*, Phys. Rev. B **82**, 104522 (2010).
- [30] T. V. Filippov *et al.*, IEEE Trans. Appl. Supercond. **13**, 1005 (2003); A. Maassen van den Brink *et al.*, New J. Phys. **7**, 230 (2005).
- [31] C. Rigetti, A. Blais, and M. Devoret, Phys. Rev. Lett. **94**, 240502 (2005); Yu-xi Liu *et al.*, Phys. Rev. Lett. **96**, 067003 (2006); G. S. Paraoanu, Phys. Rev. B **74**, 140504(R) (2006); C. Rigetti and M. Devoret, Phys. Rev. B **81**, 134507 (2010).
- [32] Yu. Makhlin *et al.*, Nature **398**, 305 (1999); J. Q. You *et al.*, Phys. Rev. Lett. **89**, 197902 (2002).
- [33] A. D'Arrigo *et al.* NJP **10**, 115006 (2008).
- [34] E. Paladino *et al.*, Physica Scripta **T137**, 014017 (2009).
- [35] E. Paladino *et al.*, Phys. Rev. Lett. **88**, 228304 (2002).
- [36] Y. M. Galperin *et al.* Phys. Rev. Lett. **96**, 097009 (2006).
- [37] T. Yu, J. H. Eberly, Phys. Rev. Lett. **97**, 140403 (2006).
- [38] F. Nguyen, Thesis, Paris 6 University, 2008.
- [39] C. Cohen-Tannoudji, J. Dupont-Roc and G. Grynberg, Atom-Photon Interactions, Wiley-Interscience (1993).
- [40] E. Paladino *et al.* Physica E **42**, 439 (2010).
- [41] J. L. M. Cortez, "Application of unitary transformations to fourth order perturbation theory", NASA Technical note D-3441, May 1966.
- [42] M. Abramowitz, I. A. Stegun *Handbook of Mathematical Functions*, Dover (1965).
- [43] E. Paladino *et al.*, Phys. Rev. B **81**, 052502 (2010).
- [44] Yuriy Makhlin, Alexander Shnirman, Phys. Rev. Lett. **92**, 178301 (2004).
- [45] P. Zanardi and M. Rasetti, Phys. Rev. Lett. **79**, 3306 (1997).
- [46] V. Bouchiat *et al.*, Physica Scripta **T76**, 165 (1998); Y. Nakamura *et al.* Nature **398**, 786 (1999).
- [47] G. Falci *et al.*, "Decoherence in Josephson Qubits", Proceedings of the International School of Physics Enrico Fermi, Course CLI "Quantum Phenomena of Mesoscopic Systems" edited by B. Altshuler, A. Tagliacozzo and V. Tognetti, (IOS Press, Amsterdam) 2003.
- [48] J. H. Cole *et al.*, Appl. Phys. Lett. **97**, 252501 (2010).